Sodium Superionic Conductors (NASICONs) as Cathode Materials for Sodium-ion Batteries

Qingbo Zhou[a], Linlin Wang[a*], Wenyao Li[b*], Kangning Zhao[c], Minmin Liu[a], Qian Wu[a] Yujie Yang[a], Guanjie He[b], Ivan P. Parkin,[b] Paul R. Shearing[b], Dan J. L. Brett[b], Jiujun Zhang[a*] and Xueliang Sun[d]

[a] *Institute for Sustainable Energy/College of Science, Shanghai University, Shanghai 200444, China.*

[b] *Electrochemical Innovation Lab, Department of Chemical Engineering, University College London, London WC1E 7JE, United Kingdom.*

[c] *Laboratory of Advanced Separations (LAS) École Polytechnique Fédérale de Lausanne (EPFL) Sion CH-1950, Switzerland.*

[d] *Department of Mechanical and Materials Engineering, University of Western Ontario, 1151 Richmond St, London, Ontario, N6A 3K7, Canada.*

E-mails: wlinlin@mail.ustc.edu.cn; wenyao.li@ucl.ac.uk; jiujun.zhang@i.shu.edu.cn

Abstract: Sodium-ion batteries (SIBs) have developed rapidly owing to the high natural abundance, wide distribution, and low cost of sodium. Among the various materials used in SIBs, sodium superion conductor (NASICON)-based electrode materials with remarkable structural stability and high ionic conductivity are one of the most promising candidates for sodium storage electrodes. Nevertheless, the relatively low electronic conductivity of these materials makes them display poor electrochemical performance, significantly limiting their practical application. In recent years, the strategies of enhancing the inherent conductivity of NASICON-based cathode materials have been extensively studied through coating the active material with a conductive carbon layer, reducing the size of the cathode material, combining the cathode material with various carbon materials, and doping elements in the bulk phase. In this paper, we review the recent progress in the development of NASICON-based cathode materials for SIBs in terms of their synthesis, characterization, functional mechanisms and performance validation/optimization. The advantages and disadvantages of such SIB cathode materials are analyzed, and the relationship between electrode structures and electrochemical performance as well as the strategies for enhancing their electrical conductivity and structural stability are highlighted. Some technical challenges of NASICON-based cathode materials with respect to SIB performance are analyzed, and several future research directions are also proposed for overcoming the challenges toward practical applications.

Keywords: Sodium-ion battery; Cathode materials; Energy storage; Sodium superionic conductor (NASICON)

1. Introduction

With the rapid increase in energy demand, the fast consumption and depletion of fossil fuels as well as the increase in environmental pollution have become concerns in recent years [1-4]. To mitigate and develop alternative solutions to the energy supply, new clean energy sources, such as solar, wind, falling water, and sea waves, have been identified as sustainable candidates for electrical energy generation [5,6]. To fully utilize such weather-dependent and intermittent electrical energy, the development of energy storage technologies, such as batteries, supercapacitors, and water electrolysis for hydrogen generation, is necessary [7-9]. Regarding batteries, lithium-ion batteries (LIBs) have high energy/power densities, relatively long lifespans, and are environmentally friendly; thus, they have been extensively developed and commercialized [10-15]. However, lithium has a natural reserve of only 0.0065% in Earth's crust, which is not enough for large-scale and sustainable commercialization [16,17]. Therefore, research on sodium-ion batteries (SIBs) has been increasing and has become a hot research topic due to the plentiful natural abundance and low cost of sodium on Earth [18-24].

Regarding SIBs, cathode materials play a critical role in energy/power densities and cycle life [25]. Currently, the most widely studied SIB cathode materials are layered transition metal oxides [26-32] and polyanions [33-37]. For example, layered transition metal oxides, such as $NaCoO_2$ [38,39] and Na_xMnO_2 [40], exhibit fast Na^+-ion insertion/extraction reactions, but the materials undergo significant structural changes and bulk expansion during the charge/discharge processes of SIBs. These structural changes are due to the absence of structural stability, resulting in rapid decreases in the cycle life and cell voltage. Polyanion materials with an open three-dimensional frame structure show high potential for use in SIBs [35,41-45]. The

typical polyanion material has superionic conductivity for Na^+ ions; thus, this material is called a sodium superionic conductor (NASICON). The total formula of NASICON-type materials can be described as $Na_xMM'(XO_4)_3$ (M or M' = V, Fe, etc. X = P or S, $_X$ = 0~4). The unit structure consisting of angular sharing MO_6 ($M'O_6$) and polyhedral XO_4 groups can provide Na^+-ion diffusion channels. This frame structure helps the sodium ions spread reversibly and rapidly in the bulk phase of the material without an obvious volume change in the main structure of the crystal. Among NASICON-type SIB cathodes, $Na_3V_2(PO_4)_3$ and $Na_3V_2O_{2x}(PO_4)_2F_{3-2x}$ have been well studied. However, the relatively low electronic conductivities of such materials make them display poor electrochemical performance, which significantly limits their practical application. To implement additional research studies, this review summarizes recent research progress in NASICON-type SIB cathode materials with a focus on the material synthesis, characterization, functional mechanism and electrochemical performance validation/optimization. Several technical challenges in developing NASICON-type cathode materials are proposed, and possible research directions are also analyzed to overcome the challenges of using NASICON-type cathode materials in practical applications.

2. NASICON-type cathode materials

2.1 Charge and discharge processes of sodium-ion batteries

The working principle of sodium-ion batteries (SIBs) is very similar to that of lithium-ion batteries (LIBs). Basically, the Li^+ ions in LIBs are replaced by Na^+ ions, and the mutual conversion between chemical energy and electrical energy is realized by the insertion and extraction of Na^+ ions between the cathode and anode electrode

materials. In this regard, the working principle of SIBs is similar to that of LIBs except that the Li^+ ions involved in the insertion and extraction reaction are replaced by Na^+ ions. As shown in **Fig. 1a**, when the SIB is charged, an oxidation reaction takes place on the cathode electrode, with Na^+ ions deintercalating from the cathode electrode, passing through the electrolyte-saturated separator, and subsequently intercalating into the anode electrode; the electrons travel through an external circuit to the anode and form a sodium metal adduct to complete the charge process. When the SIB is discharged, the anode is oxidized with Na^+ ions released from the anode material into and passing through the electrolyte separator and inserted into the cathode with electrons traveling through an external circuit to the cathode, forming a Na^+ ion-containing cathode material to complete the discharge process.

2.2 NASICON-type $Na_3V_2(PO_4)_3$ cathode materials

Among numerous NASICON-type materials, $Na_3V_2(PO_4)_3$ (NVP) is one of the most representative cathode materials [46-48]. The three-dimensional skeletal structure of NVP makes it exhibit high thermal/chemical stability. Compared to other transition metal materials with NASICON structures, NVP has the advantages of easy preparation, large capacity and a high voltage window. These excellent features make NVP a very promising material in SIB applications. However, the low conductivity of this material can lead to poor rate performance and low cycling stability as SIB cathodes [49,50]. Therefore, many strategies have been proposed and carried out to solve this issue, as shown in **Fig. 1b**. These strategies include reducing the NVP particle size, coating NVP particles with a conductive carbon layer or transition metal oxide, combining NVP particles with various carbon materials and doping other ions

to increase charge carrier transport kinetics. These strategies are beneficial to improving the surface conductivity and bulk phase conductivity. The intrinsic conductivity of NVP is usually adjusted by ion doping. In this section, these strategies for improving NVP conductivity will be presented in terms of the NVP crystal structure, reaction mechanisms, and surface/bulk structure modifications for increasing performance as SIB cathodes.

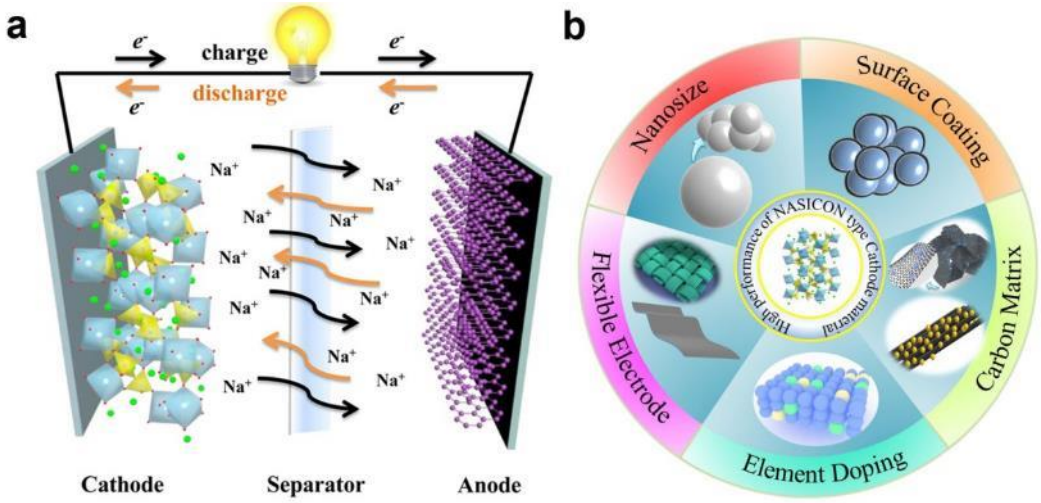

Fig. 1 a Schematic showing the charge and discharge processes of a sodium-ion battery (SIB). **b** Strategies for improving the conductivity of NASICON-type SIB cathode materials.

2.2.1 Crystal structure and storage mechanism of NVP

NVP has a three-dimensional open frame structure with a rhombic crystal structure and a space group of $R\bar{3}c$ [51]. Its primitive cell is composed of a VO_6 octahedron and PO_4 tetrahedron, which share oxygen atoms at the vertex and connect to each other to form the basic $[V_2(PO_4)_3]$ skeleton unit. Each formula unit may contain up to four univalent sodium ions. **Fig. 2a** shows that there are two types of sodium ions with oxygen atom coordination in the crystal of NVP: Na1 (6b sites) and Na2 (18e

sites). By analyzing the spatial structure of the two active sites, it can be concluded that the space at the Na1 site is smaller and that sodium ions may not be able to reversibly intercalate or deintercalate. Therefore, only Na2 ions in the crystal of NVP have electrochemical activity. **Fig. 2b** reveals the possibility of the migration scheme of Na^+ ions. This scheme can reasonably explain the theoretical specific capacity of 117.6 mAh g^{-1} for NVP. In this regard, Song et al. [52] used the first-principles theory and calculated the activation energy of NVP and obtained the migration energy of Na^+ ions with different diffusion paths in the crystal during the charging and discharging processes. The three possible Na^+ ion diffusion paths are shown in **Fig. 2c**. The first diffusion path is that Na^+ ions pass through the channel between two PO_4 tetrahedrons and diffuse along the x-axis. The corresponding migration energy is 0.0904 eV. The second diffusion path is that Na^+ ions diffuse along the y-axis through the gap between the PO_4 tetrahedron and VO_6 octahedron, and the corresponding migration energy is 0.11774 eV. The third diffusion path is that Na^+ ions diffuse through the channel between the adjacent PO_4 tetrahedron and VO_6 octahedron and diffuse along the z-axis, and the corresponding migration energy is 2.438 eV. Jian et al. [51,53] studied the reaction mechanism of NVP by both in situ XRD (**Fig. 2d**) and spherical aberration correction TEM (**Fig. 2e**) and further analyzed the crystal structure during the electrochemical reaction process. There were two different occupancies of sodium sites: 6b sites (Na1, M1) and 18e sites (Na2, M2) in the $Na_3V_2(PO_4)_3$ crystal cell. These results suggested that there were two typical phase reactions in the process of charging and discharging. Only sodium atoms occupying M2 sites could be deintercalated, indicating that two sodium atoms were able to be deintercalated from the NVP structure. The volume change of the crystal in the reaction process was 8.26%. **Fig. 2e** shows the ABF-STEM images of $Na_3V_2(PO_4)_3$ (upper left) and

$NaV_2(PO_4)_3$ (upper right) along with the [111] projection; additionally, their corresponding line profiles are under the images. In the ABF-STEM image of $NaV_2(PO_4)_3$, no sodium atom occupies the M2 sites, whereas a Na atom is visible in the ABF-STEM image of $Na_3V_2(PO_4)_3$. The corresponding red line profiles were also studied by inverting the image contrast of the dark dots and displaying them as peaks. The results show only one peak instead of the two obvious peaks of sodium atoms in $Na_3V_2(PO_4)_3$. However, there is no peak that can be observed in the corresponding sites of $NaV_2(PO_4)_3$, suggesting that although there are numerous vacancies, Na atoms cannot completely occupy the M2 sites of $Na_3V_2(PO_4)_3$. This result confirms the previous view that the storage mechanism of sodium ions in the NVP structure is a two-electron reaction system; that is, only sodium ions at the Na2 sites participate in the reaction, while sodium ions at the Na1 sites are inert and do not participate in the reaction.

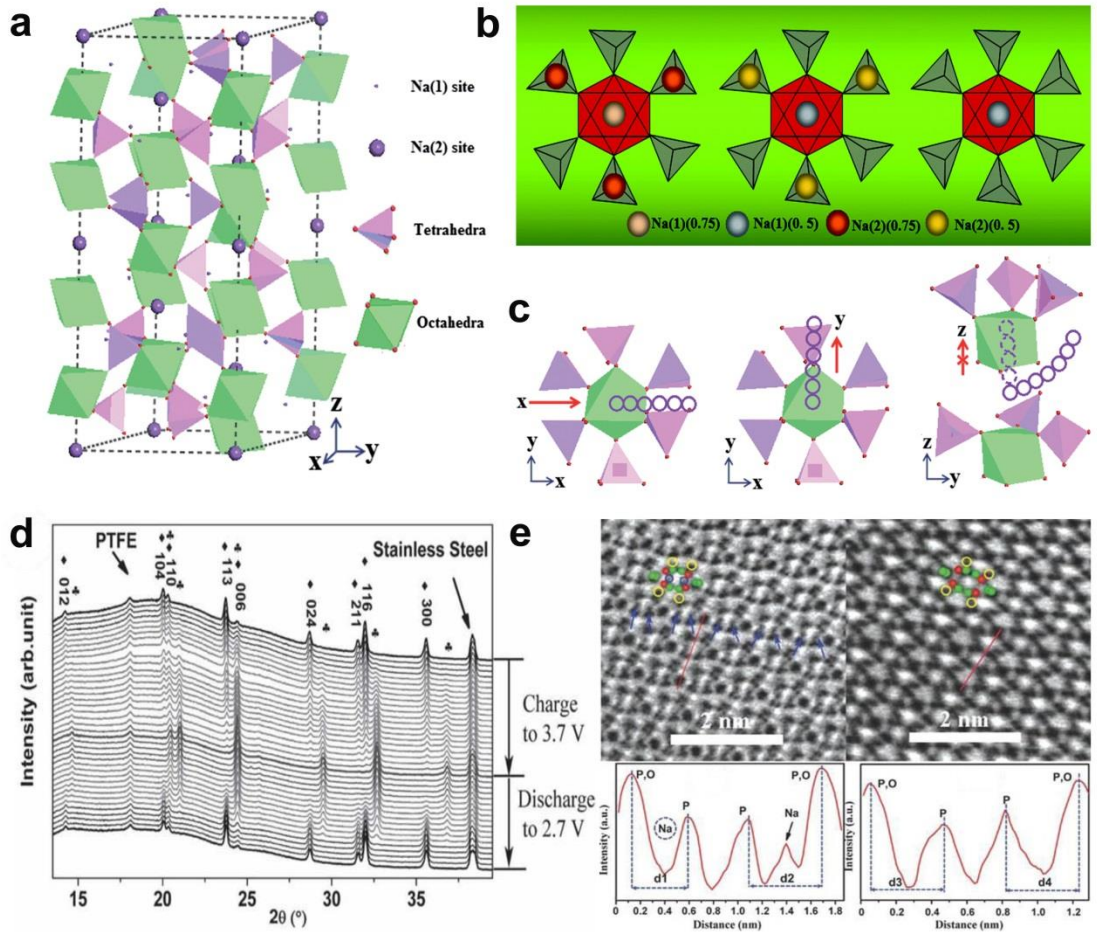

Fig. 2 **a** Crystal structure of $Na_3V_2(PO_4)_3$, **b** Na^+ ion occupation based on the calculated $[Na_3V_2(PO_4)_3]_2$ unit mode. **c** Possible Na^+ ion migration paths along the x, y, z directions [52]. Copyright 2014, Royal Society of Chemistry. **d** In situ XRD patterns of $Na_3V_2(PO_4)_3$ during the charge/discharge processes [53]. Copyright 2013, WILEY-VCH. **e** Projection for $Na_3V_2(PO_4)_3$ and $NaV_2(PO_4)_3$ along the (111) plane (the blue and yellow circles are Na atoms at the M1 and M2 sites, respectively, the blue arrow represents Na atoms at the M2 site.) and the red line curves are from the inverted image contrast of the dark dots in the ABF images [51]. Copyright 2014, WILEY-VCH.

2.2.2 Strategies for improving the performance of NVP

As mentioned previously, NASICON-type cathode materials have the advantages of a

stable structure, high working voltage and good thermal stability. However, the low conductivity of these materials limits their electrochemical performance. In view of this, researchers usually adopt many strategies to improve the conductivity to enhance their rate performance and cycle life, such as size reduction, surface coating, ion doping and designing three-dimensional flexible electrodes[54-57].

2.2.2.1 Nanocrystallization

Usually, the cathode material in a battery is not fully involved in the electrochemical reaction because of the existence of dead corners. For a cathode material, the larger the particle size, the more dead corners that cannot participate in the reaction, resulting in larger capacity loss. In addition, larger particles can also result in a lower tap density and a lower energy density. Moreover, the synthesis process of NVP inevitably involves high-temperature calcination, in which the precursor particles can form large secondary particles or even bulk materials, which can seriously affect the rate of ion diffusion and prevent the improvement in electrochemical performance. Therefore, reducing the particle size of the NVP material should be an effective way to improve the capacity and energy density [58-60]. With this approach, the diffusion distance of Na^+ ions can be reduced in the solid phase, and the active sites of Na^+ ion exchange with electrons and electrolyte can also be increased, therefore leading to an NVP material with enhanced electrochemical behavior.

Duan et al. [54] prepared NVP-based composites (NVP@C nanoparticles) by a sol-gel-assisted hydrothermal method. The morphology of this product was nanoparticles with a radius of approximately 30 nm. **Fig. 3a-c** displays the schematic diagram of the model for both ion and electron conductance. By studying and contrasting the electrochemical characteristics of large-sized NVP and NVP/C particles and NVP@C nanoparticles, they found that the large-sized NVP particles

had an unfavorable diffusion distance for Na^+ ions in the bulk phase due to the larger particle size. The redox reaction could only occur in the outer layer of the bulk phase; thus, electron conduction was also impeded. For large-sized NVP/C particles, although the coated carbon could enhance the conductivity, most of the particles were in an inactive state. However, NVP@C nanoparticles exhibited a much higher conductivity. **Fig. 3d** shows the corresponding *dQ/dV* plots. The oxidation and reduction peaks of the three samples attributed to the V^{4+}/V^{3+} redox couples can be clearly seen. Notably, NVP@C nanoparticles exhibit the most highly symmetrical sharp peaks with a small potential polarization (ΔE) value of 31 mV. Such a small ΔE exactly proves the lower polarization of the electrode and fast migration of Na^+ ions, which can be attributed to the effects of the nanosized particles and conductive coating. The cyclic performances of the three samples at 0.5C are compared in **Fig. 3e**. After 50 charge and discharge cycles, the capacity retentions of the NVP@C nanoparticles, large-sized NVP/C, and NVP are 99.6%, 87.6%, and 63.6%, respectively. This result indicates that small nanosized particles can realize the high utilization of active materials; thus, enhanced electrochemical performance is achieved.

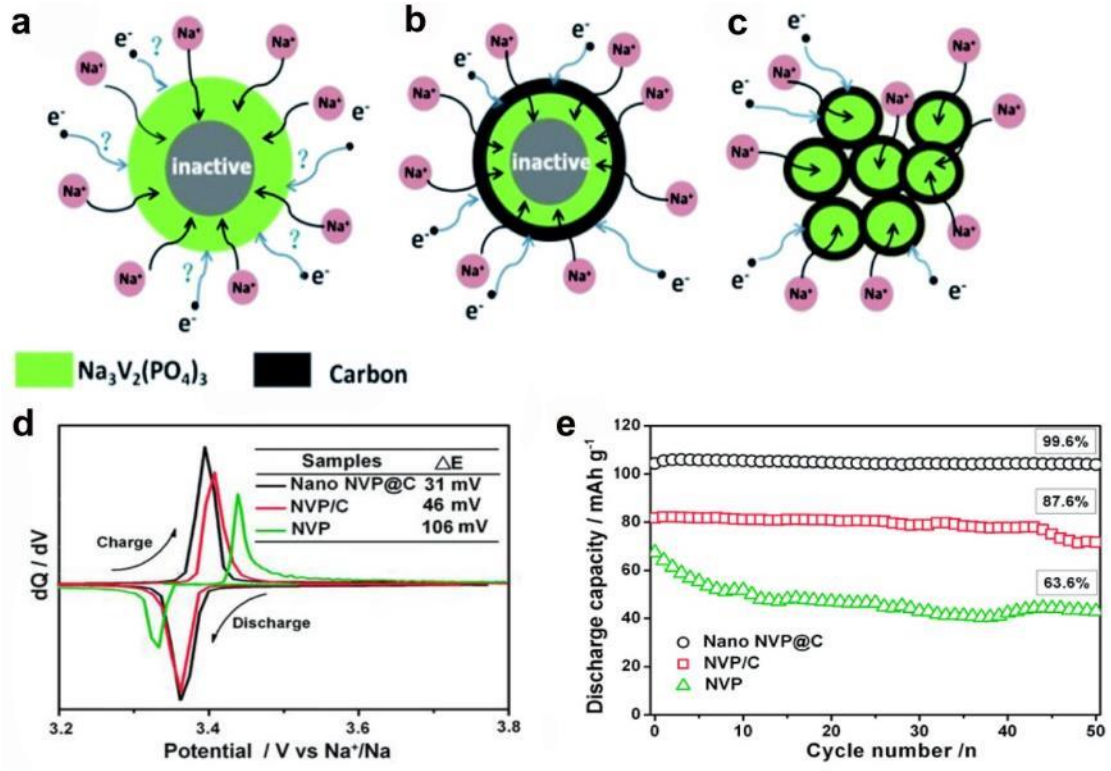

Fig. 3 Schematic diagram of electron conduction and Na^+ ion transport paths within **a** large-sized NVP, **b** large-sized NVP/C, and **c** NVP@C nanoparticles. Electrochemical properties of **d** the corresponding *dQ/dV* plots and **e** cyclic performance of different cathodes at 0.5C [54]. Copyright 2014, Royal Society of Chemistry.

In the synthesis of nanomaterials, surfactants are often used to adjust the morphology and size of the product. Jiang et al. [61] synthesized one-dimensional NVP nanowires with a mesoporous core-shell structure (NVP@C-CNW) by controlling the amount of cetyl trimethyl ammonium bromide (CTAB), as shown in **Fig. 4a**. This material shows a large specific surface area that can fully contact the electrolyte. It can reduce the diffusion distance of Na^+ ions, conduct electrons and transfer ions while also having enough space for volume expansion in the course of repeated charge and discharge cycling. In addition, its core-shell structure can effectively inhibit the formation of larger particles over the course of the annealing

process and ultimately form nanoparticles inside the nanowires. This nanowire structure also increases the electronic conductivity of NVP and improves the rapid charging performance. Therefore, NVP@C-CNW shows excellent rate performance (62.2 mAh g^{-1} at 60C) and a superlong lifespan (96 mAh g^{-1} after 1000 cycles at 1C and 74.4 mAh g^{-1} after 1000 cycles at 20C with a low decay of 1.79% per cycle, as shown in **Fig. 4b-c**). Yu et al. [62] prepared NVP@C-N nanoparticles through a facile hydrothermal-assisted sol-gel route. During the synthesis process, they used PEG-400 as the surfactant to adjust the particle size. The obtained product (NVP@C-N150) delivered both excellent rate performance and cycle life. Even at a high rate of 80C, NVP@C-N150 could reach a specific capacity of up to 71 mAh g^{-1}, while the specific capacity of NVP@C was below 20 mAh g^{-1}. From these studies above, it can be concluded that surfactants can not only be selected as an effective way to adjust the size of the product but also be used as the carbon source to produce a carbon layer on the NVP product after carbonization, efficiently preventing agglomeration between particles.

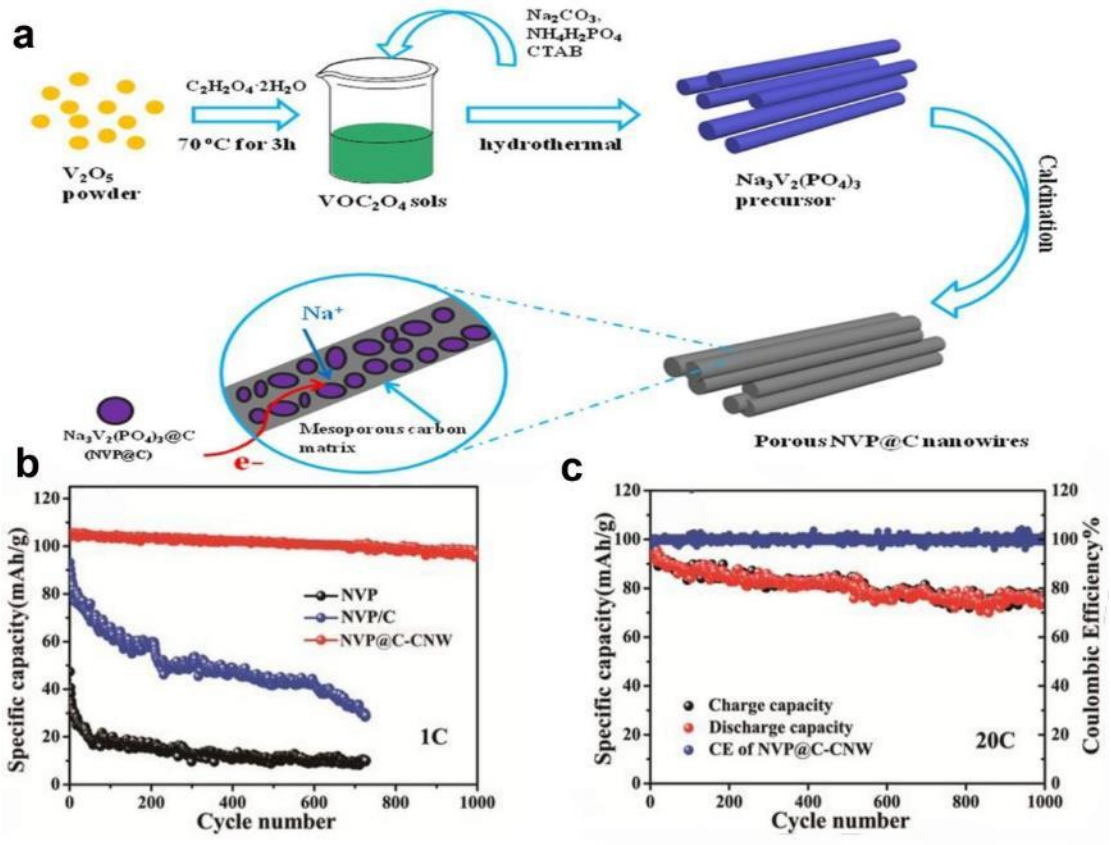

Fig. 4 a Schematic showing the experimental process to fabricate NVP@C-CNW. **b** Cycling performance of all samples at 1C for 1000 cycles, **c** specific capacity of NVP@C-CNW at a rate of 20C for 1000 cycles and the coulombic efficiency of NVP@C-CNW for 1000 cycles at 20C [61]. Copyright 2016, Wiley-VCH.

2.2.2.2 Surface coating

(1) Heteroatom-doped carbon coating

The most commonly used surface coating strategy is to coat active substances with a conductive carbon layer or metal oxide [63-65]. These two types of coatings can give the substrate material different performances. First, for pure-phase NVP materials, the conductivity is generally low. In this case, coating the surface of active material with amorphous carbon can increase its conductivity to improve electrochemical performance. In recent years, the heteroatom doping of nitrogen (N), phosphorus (P),

boron (B) and sulfur (S) into carbon materials has been proven to be an effective strategy to adjust their electrical properties [66-70]. Heteroatom doping can introduce a large number of external defects and active sites to enhance the electronic conductivity of carbon materials and decrease the energy barrier of ion penetration. Among these heteroatoms, nitrogen is the most widely studied because nitrogen doping can generate external defects, leading to enhanced reactivity and electrical conductivity. Jiang et al. [71] designed 3D flower-like $Na_3V_2(PO_4)_3$ composites coated with N, B codoped carbon (NVP@C-BN), as shown in **Fig. 5a**. The special architecture and large available area of this material can facilitate both Na^+ ion diffusion and electronic transport (**Fig. 5b**). NVP@C-BN also demonstrates excellent electrochemical properties (**Fig. 5c),** indicated by its better cycle life than NVP@C even at a high rate of 20C. In addition, as shown in **Fig. 5d**, this material can deliver an outstanding rate capability when compared to that of NVP@C. NVP@C-BN has an outstanding capacity even at 100C (84 mAh g^{-1} can be retained). XPS analysis was also conducted to reveal the mechanism of the doping effect of B and N. Several combinations, namely, B_4C, BC_3, N-B, BC_2, and BCO_2 exist after doping, and BC_3 is found to be able to enhance the conductivity of the carbon layer. The other types produce a large number of defects and active sites in the carbon layer and boost Na^+ ion absorption and ultrafast Na^+ ion diffusion on the surface of carbon during the electrochemical reaction. Therefore, the electrochemical performance can be significantly improved.

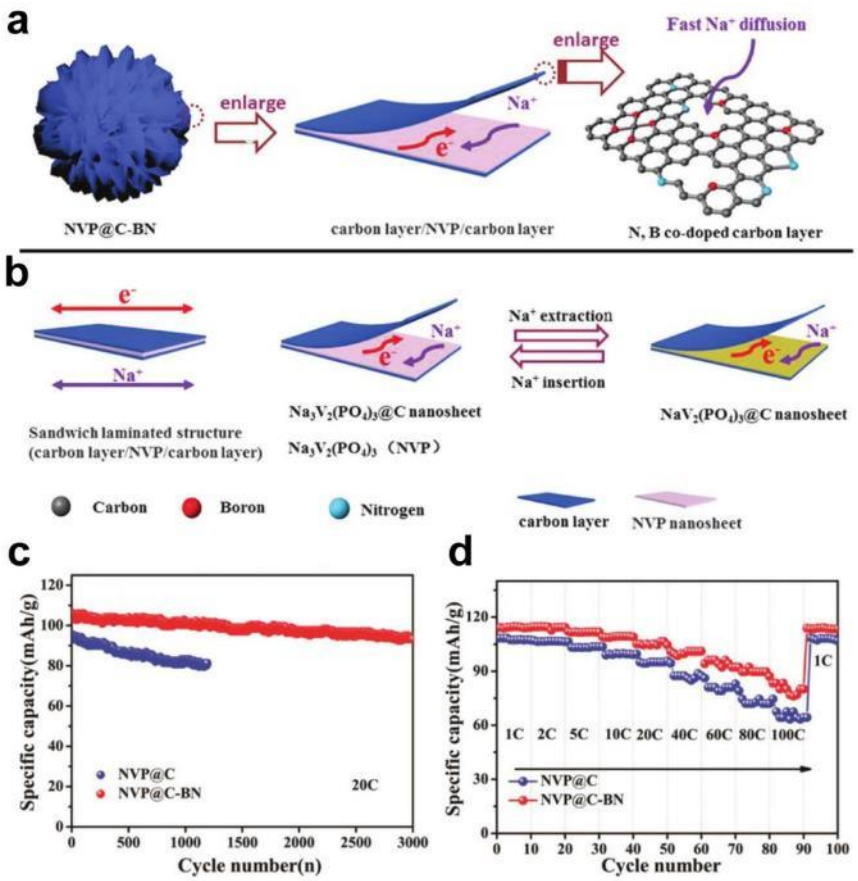

Fig. 5 a Schematic diagram showing the structure of NVP@C-BN. **b** Na diffusion pathway and electron conduction in the material. **c** Lifespan of NVP@C and NVP@C-BN at 20 °C for 3000 cycles. **d** Rate capacities of the two electrodes from 1-100 °C [71]. Copyright 2018, WILEY-VCH.

(2) Coating with metal oxides

Normally, contact between the active substance and electrolyte can cause side reactions during the charging and discharging processes of batteries [72]. These reactions will result in the generation of HF and other substances in the electrolyte and cause corrosion of the active material. If the cathode material is coated with a metal oxide on the surface, the hydrogen fluoride in the electrolyte can be at least partially neutralized by the conversion of the metal oxide into fluoride, thereby greatly reducing the acidity of the electrolyte and delaying cathodic corrosion during

cycling [73]. In this regard, Klee et al. [73] prepared $Na_3V_2(PO_4)_3$ by the sol-gel method and then deposited carbon and M_xO_y (M_xO_y =Al_2O_3, MgO or ZnO) onto the surface of such a material by ultrasonic stirring technology, as shown in **Fig. 6a, c**. XPS and TEM measurements confirmed the successful coating of M_xO_y on the $Na_3V_2(PO_4)_3$ surface to form C+M_xO_y@$Na_3V_2(PO_4)_3$. According to **Fig. 6b**, the capacity and stability of the sample coated with 1.5% metal oxide can be significantly improved.

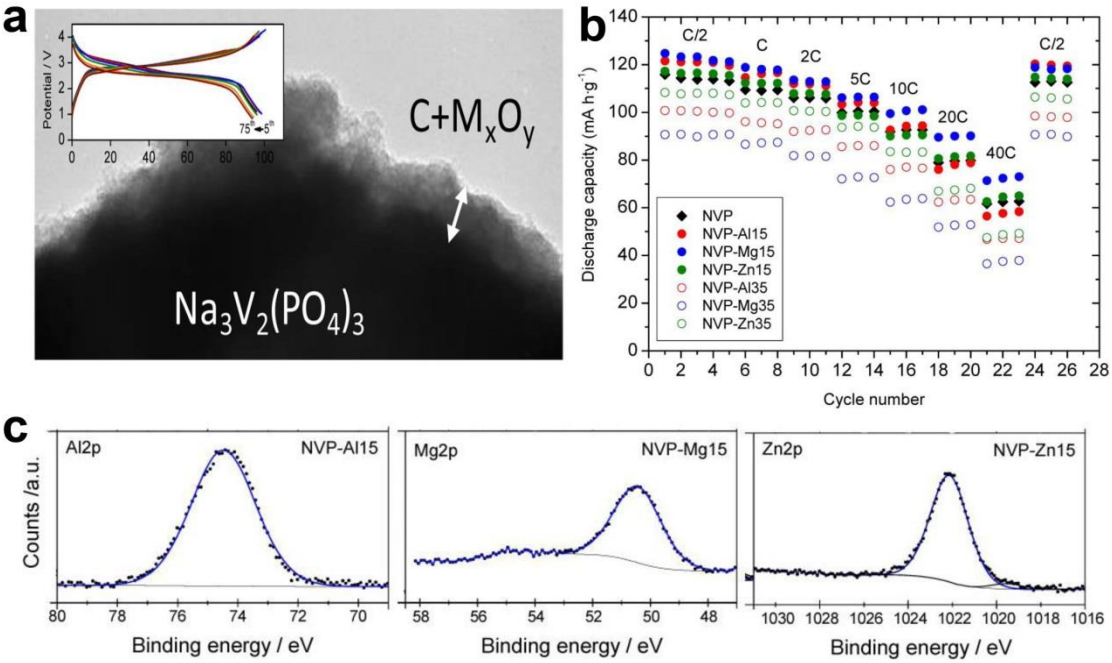

Fig. 6 a TEM image and **b** rate capability of C+M_xO_y@$Na_3V_2(PO_4)_3$. **c** XPS spectra of the electrodes (M_xO_y =Al_2O_3, MgO or ZnO) [73]. Copyright 2016, American Chemical Society.

2.2.3 Hybrid with different kinds of carbon materials

Compositing conductive carbon-based materials with NVP precursors can also improve the electrical conductivity of NVP. In this regard, graphene is a kind of two-dimensional carbon nanomaterial with a hexagonal shape and honeycomb lattice

formed by carbon atoms with sp^2-hybridized orbitals. Because of its excellent optical, electrical, and mechanical properties, graphene is widely used as a composite/loaded matrix material for electrode materials, similar to other highly conductive carbon substrates, such as carbon nanotubes [74-77]. Rui et al. composited reduced graphene (rGO) with NVP and obtained 3D hierarchical meso- and microporous NVP@C@rGO nanocomposites using a simple freeze-drying-assisted method, as shown in **Fig. 7a, b** [78]. The obtained NVP@C@rGO cathode shows both excellent rate capacity (86 mAh g^{-1} at 100C) and long cycling life (retained 64% after 10000 cycles at 100C). Hen et al. [79] prepared NVP microspheres modified with carbon nanotubes (CNTs) as a cathode material by using spray drying combined with the carbon thermal reduction method. As shown in **Fig. 7c**, the microspheres are encased and embedded by carbon nanotubes, and the surface is also wrapped by an amorphous carbon layer, revealing that a carbon network consisting of CNTs is formed in the material. **Fig. 7d** shows that at 0.5C, the electrode has a capacity of 103.2 mAh g^{-1}, and when increased to 20C, the discharge capacity is as high as 91.2 mAh g^{-1}. Even at a high current density of 60C, the capacity is still approximately 80 mAh g^{-1}. These results demonstrate that the carbon nanotube modification can reduce the resistance of the material. Compared with the original NVP electrode without CNTs, the polarization of the 10 wt% CNT-modified NVP (NVP/C10) electrode is much smaller. Furthermore, the addition of CNTs can adjust the NVP particle size, increasing the contact area of NVP with the electrolyte and the Na^+-ion diffusion coefficient.

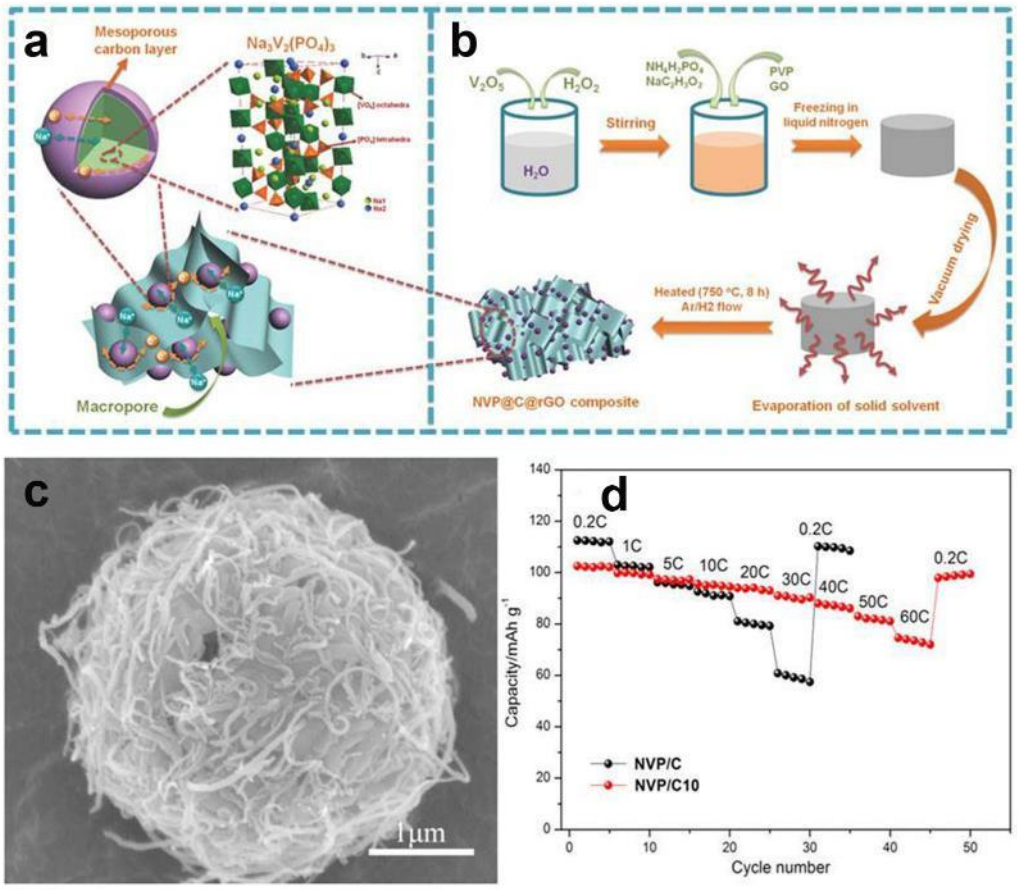

Fig. 7 a Schematic of NVP@C@rGO including pathways for both electrons and Na^+ ions and the crystal structure. **b** Schematic of the freeze-drying-assisted method to fabricate the NVP@C@rGO composite [78]. Copyright 2015, WILEY-VCH. **c** SEM images and **d** rate performance of CNT-decorated NVP [79]. Copyright 2018, American Chemical Society.

In addition to compositing with highly conductive graphene or carbon nanotubes, NVP can also be composited with highly ordered mesoporous carbon, which is named the CMK-3 substrate (NVP@C@CMK-3) [80]. As demonstrated by Jiang et al. [81], CMK-3 is an ideal template for the synthesis of mesoporous carbon matrix composite electrode materials. They used a mesoporous molecular sieve (SBA-15) as a template to prepare CMK-3 mesoporous carbon, as shown in **Fig. 8a**. In their synthesis,

glucose is mixed with the raw material precursor to achieve the surface carbon coating of NVP. After calcination in CMK-3, the two-dimensional core-shell-structured NVP@C@CMK-3 is obtained. As the cathode for SIBs (**Fig. 8b**), the reversible specific capacity of NVP@C@CMK-3 is 103 mAh g^{-1}, which is 87% of the theoretical specific capacity. Even at a current density of 20C, its first discharge specific capacity can still reach 102 mAh g^{-1} while retaining 67.3% after 1000 cycles. Additionally, the coulombic efficiency is very close to 100% throughout the cycle process. This outstanding performance is attributed to the core-shell structure contained in the ordered mesoporous carbon matrix, which can be conducive not only to the rapid transmission of electrons but also to the full penetration of electrolyte, promoting the rapid transfer of Na^+ ions.

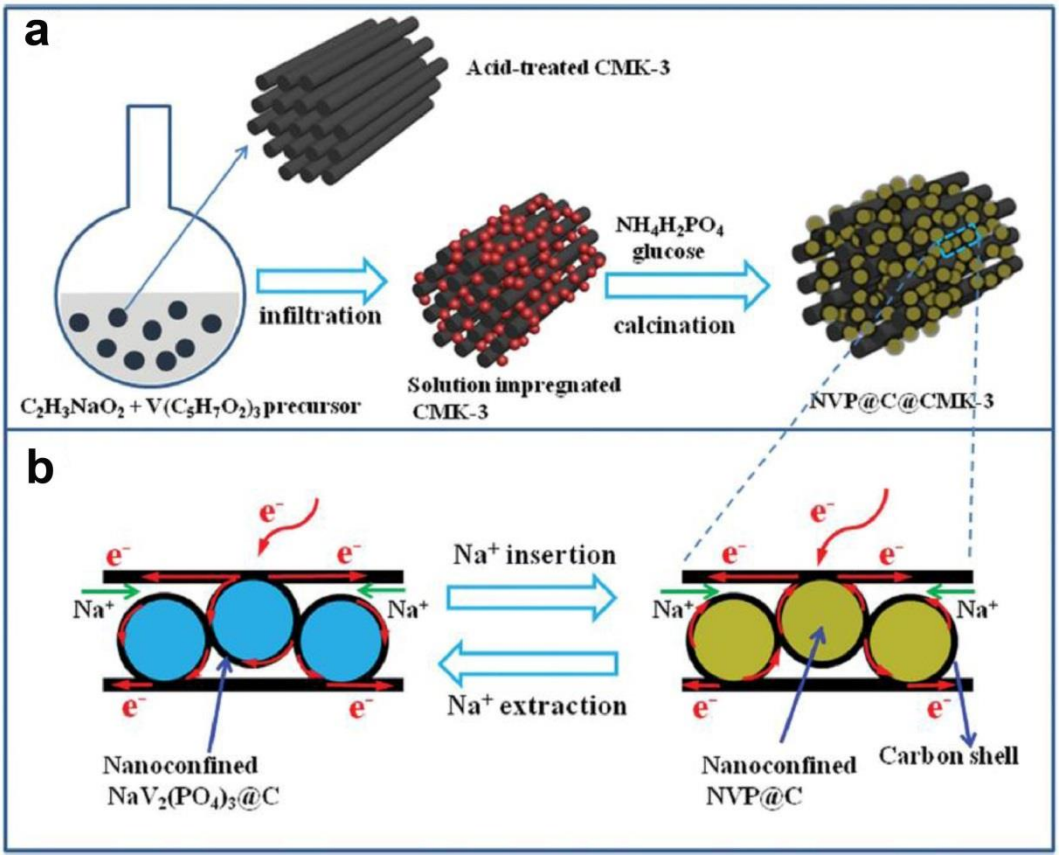

Fig. 8 a Schematic diagram showing the fabrication process of NVP@C@CMK-3 and **b** electron conduction and Na^+ ion transport process [81]. Copyright 2015, WILEY-VCH.

2.2.4 Element doping

A carbon coating cannot improve the electron conductivity of the bulk phase of active materials; however, the conductivity of the bulk phase can be improved by doping ions into the structure. At present, the doping of bulk phase NVP mainly involves the partial substitution of V, polyanion and Na positions. The Na site is generally doped with Li^+ or K^+. The V site is generally doped with transition metal elements such as Fe^{2+} [82,83], Mn^{3+} [84-86], Mg^{2+} [87, 88], Ga^{3+} [89], Ni^{2+} [90], Ca^{2+} [91], Al^{3+} [92], Cr^{2+} [93, 94], and Mo^{6+} [67]. The doping of polyanion positions commonly uses nonmetallic elements such as oxygen and fluorine [45, 95, 96].

Liu et al. [82] prepared an Fe-doped NVP@C cathode material using organic iron sources. The process is shown in **Fig. 9a**. The decomposition of organic iron can promote the formation of graphitized carbon and porous structures, facilitate the penetration of electrolyte, and shorten the diffusion distance of ions. Electrochemical measurements revealed that the rate performance and cycle life of the Fe-doped NVP/C electrode could be significantly improved. In particular, $Na_3V_{1.85}Fe_{0.15}(PO_4)_3$@C could deliver a high capacity of 103.69 mAh g^{-1}. The capacity retention could be maintained at 91.45% after 1200 cycles at 1.0C, while showing a capacity of 94.45 mAh g^{-1} at 20C. The optimal performance could be achieved when the doping amount of Fe was 1.5%. As shown in **Fig. 9b**, the cathode can stably undergo 1000 cycles at a rate of 5C while maintaining a capacity of more than 90 mAh g^{-1}. They also carried out DFT calculations and found that the most stable position of Fe atoms was the V position, and the appropriate displacement of Fe

in the V position could reduce the bandgap from 2.19 to 0.43 eV, greatly improving the conductivity of the material.

Li et al. [88] synthesized Mg-doped $Na_3V_{2-x}Mg_x(PO_4)_3$/C composites. The SEM image and rate capabilities are shown in **Fig. 9c-d**. The electrochemical performance of the materials are strongly dependent on the controlled amount of Mg^{2+} (x=0, 0.01, 0.03, 0.05, 0.07 and 0.1). Their results show that the doping of Mg^{2+} will not change the crystal structure of NVP. When the doping amount was 5%, $Na_3V_{1.95}Mg_{0.05}(PO_4)_3$/C was able to deliver an initial capacity of 106.4 mAh g^{-1} at 20C and finally stabilized at 86.2 mAh g^{-1} after 50 cycles. In contrast, the initial discharge capacity of the $Na_3V_2(PO_4)_3$/C sample was only 10 mAh g^{-1} at the same rate, which demonstrates the outstanding capacity retention of the Mg-doped $Na_3V_{1.95}Mg_{0.05}(PO_4)_3$/C composite. They also analyzed the mechanism and found that the doping of Mg^{2+} could accelerate the diffusion rate of Na^+ ions and increase the conductivity of the material, thus enhancing the electrochemical properties of the $Na_3V_{2-x}Mg_x(PO_4)_3$/C cathode material.

As identified, introducing fluorine at polyanion sites can improve the working voltage of the material because of the high electronegativity of fluorine [97]. Chen et al. reported a promising nanoscale $Na_3V_2(PO_4)_{2.93}F_{0.07}$@C composite, which was fabricated through a solid-phase method [97]. The doping of F inhibited the structural degradation of $Na_3V_2(PO_4)_3$ to $V_2(PO_4)_3$ and improved the structural stability. Their results showed that an appropriate F content could provide inductive effects, which then boosted Na^+ ion diffusion and decreased electrode polarization; as a result, the kinetic behavior of the F-doped composite was significantly improved. The HRTEM images in **Fig. 9e** suggest that F was successfully introduced into the NVP phase. Compared with the undoped NVP/C sample, the discharge capacity of the

F-0.07-NVP/C composites reaches 113 mAh g^{-1} at 10 mA g^{-1}, which is very close to the theoretical capacity (117 mAh g^{-1}). In terms of the cycling performance in **Fig. 9f**, the electrode can achieve a reversible capacity of 97.8 mAh g^{-1} and maintain 86% of the initial capacity after 1000 cycles at 200 mAh g^{-1}. This excellent electrochemical performance is attributed to the synergistic effect between the enhanced kinetic behavior and structural stability after F doping.

Moreover, doping alkali metal elements [98, 99] such as Li^+ and K^+ at Na sites instead of V sites in the NVP lattice has also been investigated. For example, Lim et al. [100] doped K^+ ions into the position of Na^+ ions in $Na_3V_2(PO_4)_3$. The radius of K^+ ions is much larger than that of Na^+ ions, resulting in an enlarged Na^+ ion diffusion channel and an increased lattice volume along the c-axis. **Fig. 9g-h** shows that the rate performance of K^+-doped NVP is greatly enhanced, especially when the doping amount is 9%; this material shows the best electrochemical performance. K-0.09-NVP/C exhibits the best rate performance, and the initial capacity is 110.8 mAh g^{-1} at 0.1C. Furthermore, they also revealed that K^+ ions did not participate in the reaction processes of the electrode, suggesting that K^+ could stabilize the structure of NVP and did not cause obvious volume changes or degradation of the lattice structure. This work provided a good strategy for widening the ion intercalation reaction channel. In addition, from these studies, the intrinsic conductivity of materials can be enhanced by element doping, thus demonstrating excellent electrochemical performance.

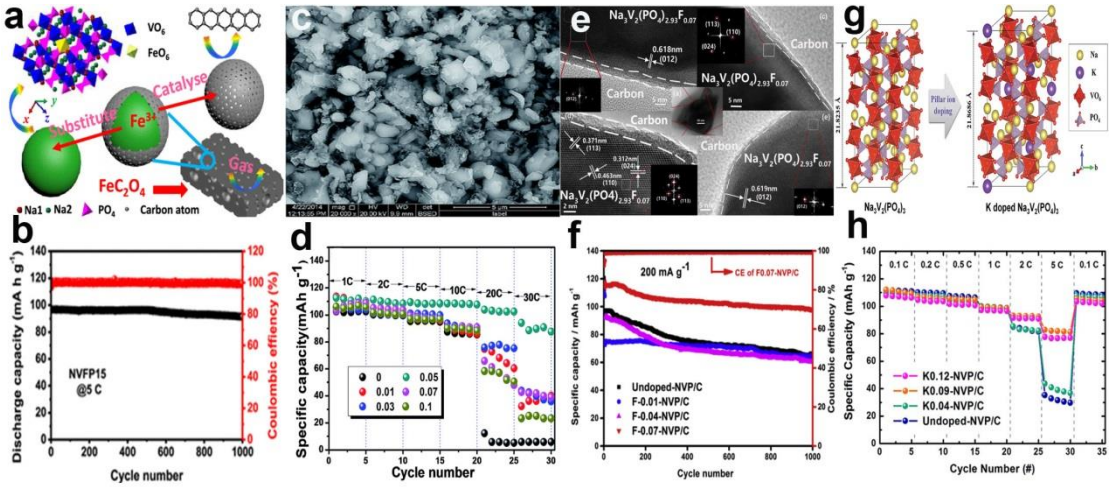

Fig. 9 a Schematic illustration of Fe^{2+}-doped NVP/C and its **b** long cycle life [82]. Copyright 2019, American Chemical Society. **c** SEM images and **d** rate capacity of Mg^{2+}-doped NVP/C [88]. Copyright 2015, Royal Society of Chemistry. **e** HRTEM image of the $Na_3V_2(PO_4)_{2.93}F_{0.07}$/C sample and the **f** long cycle life of F^--doped NVP/C [97]. Copyright 2017, Elsevier. **g** Schematic diagram showing the structural stabilization and **h** rate capacity of K^+-doped NVP/C [100]. Copyright 2014, Royal Society of Chemistry.

2.2.5 Design of three-dimensional (3D) flexible electrodes

Flexible energy storage devices have attracted increasing attention due to their flexibility, shape diversity and light weight. At the present stage, wearable watches, flexible screens, and flexible mobile phones, especially the advent of 5G folding mobile phones, have pushed the fast development of flexible batteries. To provide sufficient power to flexible wearable devices, energy storage systems should also have excellent cycling stability, good rate performance, a light weight, a low price and a high energy density. Although considerable efforts have been made to develop flexible energy storage systems [101, 102], this field is still in its early stage. The development direction of flexible batteries should consider the following three aspects: (1) can be repeatedly bent or folded without internal short circuits; (2) can maintain

good contact between the electrode, separator and electrolyte; and (3) when bending or folding, the battery should maintain a high energy density, long cycle life, and no attenuation. Therefore, improving these three aspects is the key to the evolution of flexible batteries.

There are many reported studies on flexible anodes [103-111], but few reports have focused on cathodes [13, 57, 112]. The main reasons may be the following: (1) traditional cathode electrode materials such as $LiFePO_4$ and $LiCoO_2$ have a weak ability to nucleate and grow on three-dimensional substrates; (2) most cathode materials need to be calcined at a high temperature of approximately 700-900 °C in an air atmosphere, and it is difficult for conventional substrates to maintain structure and conductivity in an air atmosphere [87]. Materials, such as those that are NVP-based, need to be calcined in an inert atmosphere during the preparation process to avoid the oxidative decomposition of their 3D carbon substrate; thus, an inert calcination atmosphere is a precondition for the preparation of flexible NVP electrode materials.

Guo et al. [113] prepared a precursor through the sol-gel method, in which the sol was dropped on a carbon cloth (CC) several times. After calcination, an NVP@C@CC flexible electrode was obtained, as illustrated in **Fig. 10a**. The loading mass of active material obtained by this method is high, and the material demonstrates favorable properties. As shown in **Fig. 10b**, the prepared NVP@C@CC electrode in a sodium half-cell displays a high rate performance of 96.8 mAh g^{-1} at 100C and 69.9 mAh g^{-1} at 200C, along with excellent cyclability and 82.0% capacity retention after 2000 cycles at 20C. Additionally, the NVP@C-CC electrode can be obtained with a higher load of active material, which also causes the cell to have a fairly high energy density of 396 W h kg^{-1} and a higher power density of 97 kW kg^{-1}.

Some researchers also tried to mix the precursor solution with polymer solution to

form a spinning solution and then prepare a flexible film by electrostatic spinning. For example, Liu et al. [114] prepared NVP@C nanofibers by electrospinning and calcination in a N_2 atmosphere, as shown in **Fig. 10c**. The morphology of the product is uniform thin nanofibers. In **Fig. 10d**, the NVP@C nanofiber electrode exhibits an initial charge capacity of 103 mAh g^{-1} and a discharge capacity of 101 mAh g^{-1} at 0.1C and retains a stable discharge capacity of 58 mAh g^{-1} at a high current density of 10C. In addition, because of the three-dimensional highly conductive network that is formed by the nanofibers of the NVP@C electrode, the transport distance of Na^+ ions is obviously shortened; thus, the electrode shows a high rate capability even when charged or discharged at high currents (up to 20C). By changing the current collection to make an integrated electrode without a binder, not only can the disadvantage of the binder on the conductivity and 'dead volume' be reduced but also the devices can be used in high power output applications.

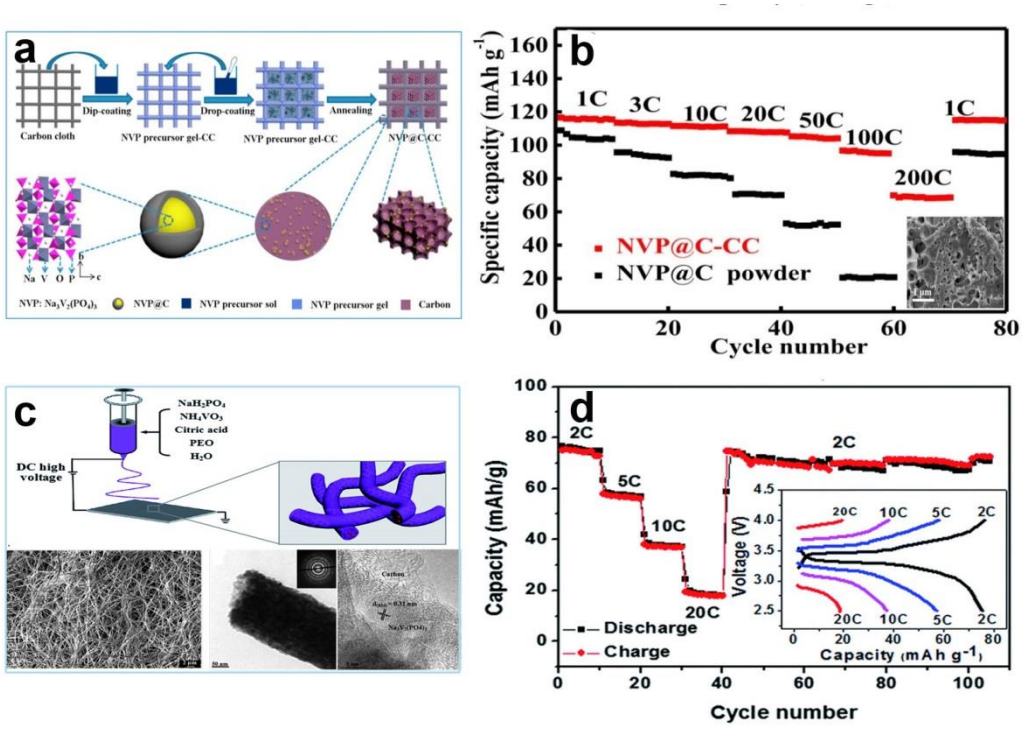

Fig. 10 a Preparation process of the NVP@C-CC electrode and **b** rate capability of

NVP@C-CC [113]. Copyright 2017, Elsevier. **c** Schematic illustration showing the synthesis process for the $Na_3V_2(PO_4)_3$/C hierarchical nanofiber and **d** rate capability of the $Na_3V_2(PO_4)_3$/C electrode [114]. Copyright 2014, Royal Society of Chemistry.

2.3 NASICON-type $Na_3V_2O_{2x}(PO_4)_2F_{3-2x}$ cathode materials

As identified, V^{3+} ions in the NVP structure cannot be oxidized into a higher valence state, making it difficult to realize whether all Na^+ ions at the Na2 site are extracted from the crystal lattice; thus, this NVP structure cannot achieve higher sodium storage performance. An effective strategy in achieving an NVP material with higher operating voltage is to enhance the bond ionicity of the anionic groups by introducing high electronegative anions (such as F^-) into the lattice to reduce the covalency of the V-O bond. This strategy increases the valence state of V (from V^{3+} to V^{4+}) and the working plateau voltage of the material. If the V-O bonds can be partly superseded by V-F, an increased redox voltage can be achieved with the valence change of V during Na^+ intercalation/deintercalation. For example, a new NASICON-structured sodium vanadium fluorophosphate can be formed after introducing F^- into the NVP lattice [115]. A type of chemical formula for this substance can be described as $Na_3V_2O_{2x}(PO_4)_2F_{3-2x}$ ($0 \leq x \leq 1$), indicating that one-third of the PO_4^{3-} in the NVP structure is replaced by F^- and O^{2-} in different proportions. The theoretical specific capacities of these materials are between 120-130 mAh g^{-1}.

2.3.1 Crystal structure and sodium storage mechanism of $Na_3V_2(PO_4)_2F_3$

The representative materials with two extreme phases of $x = 0$ and $x = 1$ are $Na_3V_2(PO_4)_2F_3$ and $Na_3(VO)_2(PO_4)_2F$, and these materials have recently attracted extensive interest for use as SIB cathodes due to their high operating voltages. When three F^- replaces one PO_4^{3-} ($x = 0$ in the general formula), the corresponding

NASICON-type $Na_3V_2(PO_4)_2F_3$ (NVPF) will have a high theoretical energy density of 507 W h kg^{-1}. The crystal structure of NVPF is relatively stable, and the working plateau voltage is enhanced due to the extremely strong electronegative property of F^-. Thus, it shows excellent electrochemical properties. Le Meins et al. [116] studied the crystal structure of NVPF and found it had the $P4_2/mnm$ space group and adopted an identical three-dimensional $[V_2(PO_4)_2F_3]^{3-}$ network consisting of PO_4 tetrahedra and $V_2O_8F_3$ bioctahedra (one apex fluorine bridges two octahedra) by sharing their corners through F; moreover, Na^+ ions were statistically distributed inside the resulting channels. Liu et al. [117] studied the local structure and kinetics of the NVPF material used for SIB cathodes. The corresponding crystal structure is presented in **Fig. 11a**. There are two-dimensional channels for Na^+ ions to insert/extract, ensuring that Na^+ ions can quickly migrate. They also studied the dynamics of ^{23}Na and proposed that there were three different electrochemical processes of NVPF during the charging process, as shown by the ex situ NMR results. The ex situ ^{23}Na NMR patterns (**Fig. 11b**) indicate that the minor resonances under 50 ppm decrease gradually in Stage I ($0<x<1.0$). The resonance intensities of Na1 and Na2 decrease at the same time, and the line width clearly becomes wider after $x = 0.3$. In Stage II ($1.0<x<1.4$) and Stage III ($1.4<x<2.0$), the Na1 resonances gradually disappear, while the Na2 resonances increase. The ex situ ^{23}Na NMR results indicate that at the Na1 and Na2 sites, there is no obvious resonance for Na deintercalation (or intercalation) during the preliminary stage of charge (or at the end of discharge), which is not consistent with earlier literature reports [118,119]. They pointed out that there are distinct Na sites in the lattice of NVPF, *i.e.*, the fully occupied Na1 site and the partially occupied Na2 site. At the beginning of the charging process, Na^+ ions are randomly extracted from both sites with no relative priority. The lattice parameter a

(=b) of NVPF will continue to increase while c gradually decreases, showing the overall characteristics of a solid-solution reaction. Bianchini et al. [120] further studied the reaction mechanism of NVPF in the electrochemical process and pointed out that a series of very complex phase transition processes could occur during Na^+-ion release. They performed operando high angular resolution synchrotron radiation diffraction measurements on SIBs during the charging progress (**Fig. 11c**), revealing that NVPF has four different intermediate phases: $Na_{2.4}VPF$, $Na_{2.2}VPF$, Na_2VPF, and $Na_{1.8\sim1.3}VPF$. Only the $Na_{1.8\sim1.3}V_2(PO_4)_2F_3$ phase undergoes a solid-solution reaction process, indicating a small volume change. A minute volume change can be detected from Na_3VPF to NaVPF, which qualifies Na_3VPF as an ideal material for long-term cycling stability. Song et al. [121] systematically studied the ion diffusion path and migration mechanism of the NVPF cathode material in SIBs by combining theoretical calculations and experimental validation. They also proposed that three Na^+ ions in each lattice cell had two Na positions. As shown in **Fig. 11d**, there are two symmetrical plateaus found in the charge/discharge curves. During charge/discharge within the voltage range of 1.6~4.6 V, both Na ions can participate in the insertion/extraction reactions, and the corresponding reaction center is the V^{3+}/V^{4+} redox transition. The average working voltage of the NVPF cathode material in the SIB is approximately 3.9 V with a theoretical specific capacity of 128 mAh g^{-1}, and the corresponding energy density is approximately 500 Wh kg^{-1}, which is higher than that of the NASICON-structured NVP cathode material (400 Wh kg^{-1}). Therefore, NVPF is a very competitive, high energy density SIB cathode material.

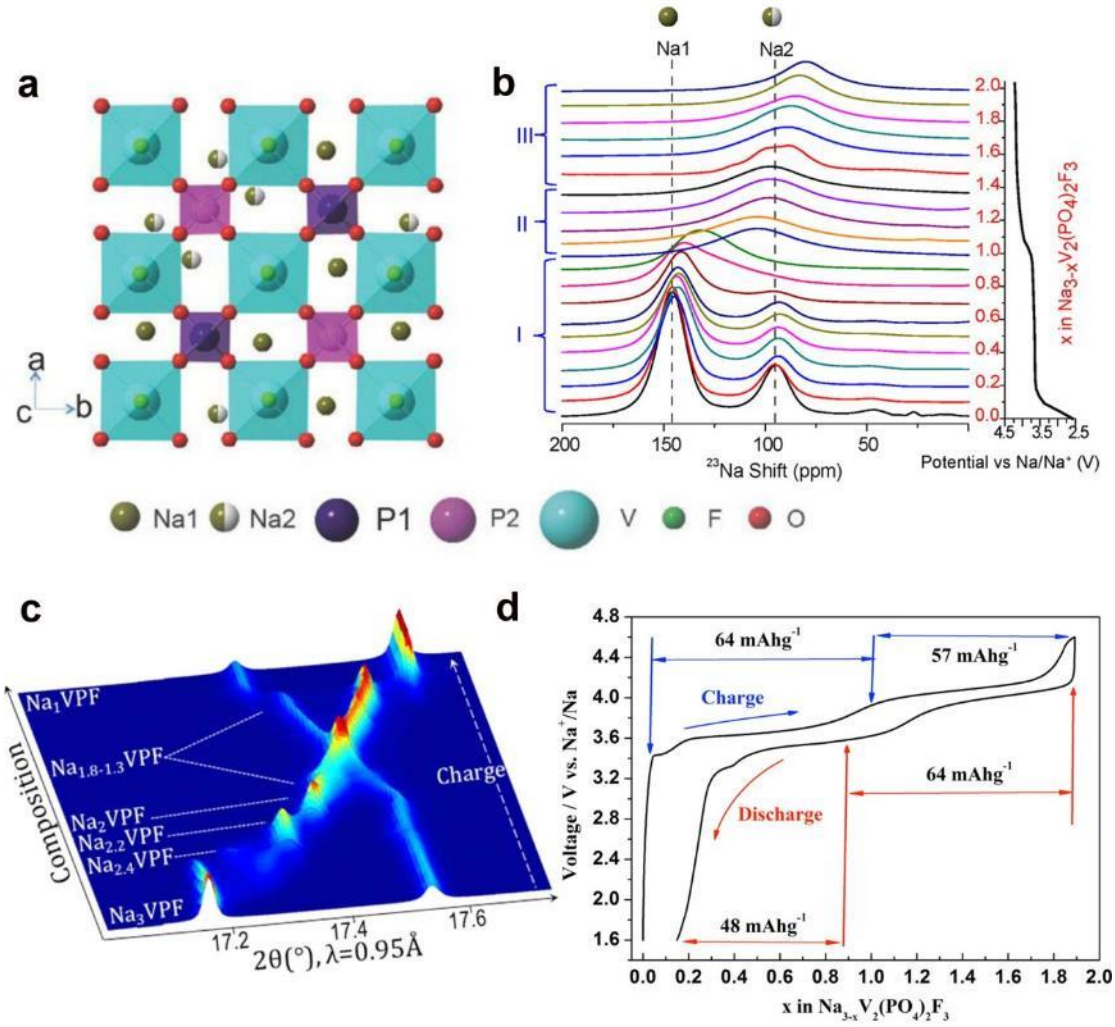

Fig. 11 **a** Schematic of the $Na_3V_2(PO_4)_2F_3$ structure projected along the c-axis. **b** Ex situ ^{23}Na NMR spectra of $Na_3V_2(PO_4)_2F_3$ electrodes at different states of charge [117]. Copyright 2014, American Chemical Society. **c** High angular resolution synchrotron radiation diffraction spectrum of the $Na_3V_2(PO_4)_2F_3$ cathode electrode [120]. Copyright 2015, American Chemical Society. **d** Electrochemical voltage-composition profile of the $Na_3V_2(PO_4)_2F_3$ sodium-ion battery at 0.91C in the voltage range of 1.6-4.6 V during the second cycle [121]. Copyright 2014, American Chemical Society.

2.3.2 Preparation and modification of the NVPF cathode material

The theoretical specific capacity of NVPF (128 mAh g^{-1}) is higher than that of NVP (117 mAh g^{-1}). In addition, the working voltage plateau is also higher than that of NVP; however, the conductivity of NVPF is just as low as that of NVP, which limits its electrochemical performance. In this subsection, the modification strategies of NVPF will be introduced with a focus on improving the conductivity of the NVPF cathode material. The modification strategies include surface coating, size reduction, combination with carbon-based materials, and bulk doping. Carbon coating for material property modification is one of the common methods to enhance the conductivity of electrode materials, being relatively simple, efficient, safe, and pollution-free [122,123]. For example, Song et al. [124] prepared NVPF@C by a carbon-thermal reduction method. The specific capacity of this material reached 115 mAh g^{-1} at 1.82C, and the capacity retention was 96% after 100 cycles. Qi et al. [125] synthesized NVPF nanoflowers by adjusting the pH value of the solution before undergoing a low-temperature hydrothermal process. As shown in **Fig. 12a-c**, the prepared NVPF nanocrystals exhibit excellent cycling stability. They were cycled 500 times at a rate of 0.2C and demonstrated a capacity retention of up to 94.5%, showing promising application prospects. Zhu et al. [126] prepared an NVPF 3D graphene conductive network (NVPF@GN) by a facile sol-gel method to improve their electrochemical properties, as shown in **Fig. 12d-e.** The particle size of NVPF after combining with the graphene conductive network was significantly smaller. Electrochemical performance tests showed that the cycling performance of

NVPF@GN significantly improved; it could reach up to 100 mAh g^{-1} even after being cycled 1000 times at a high current density of 10C, and the capacity retention was as high as 80%. The high conductivity and smaller particle size of NVPF@GN, which could be beneficial to the deintercalation/intercalation of Na^+ ions, were thought to be responsible for the improved electrochemical performance. Cai et al. [127] designed a cross-linked graphene-caged NVPF microcube (NVPF@rGO) composite through a one-pot hydrothermal method and subsequent freeze-drying and heat treatment. As an SIB cathode, NVPF@rGO exhibited outstanding cycling stability and rate performance, as well as good low-temperature adaptability. The structural evolution and diffusion kinetics during the repeated Na^+ ion deintercalation/intercalation process in the NVPF@rGO electrode were also investigated. In addition, an operational SIB full cell was fabricated using an NVPF@rGO cathode and an N-doped carbon anode. This full cell delivered excellent cycling performance with a capacity retention of 95.1% after 400 cycles at 10C, a high energy density of 291 Wh kg^{-1} and a power density of 192 W kg^{-1}. These results prove that reducing the particle size and combining with carbon-based materials are effective ways to enhance the electronic conductivity of polyanionic materials. Furthermore, they can not only enhance the conductivity of the material but also inhibit the growth of particles, reduce the agglomeration of particles, increase the solid (active particles)-liquid (electrolyte) contact area, and shorten the ion diffusion path.

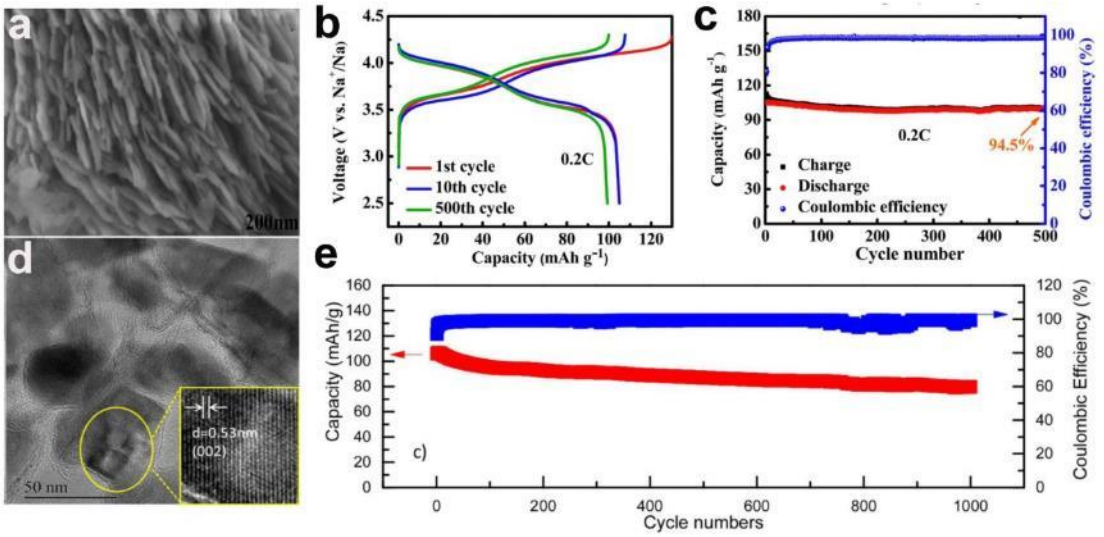

Fig. 12 **a** SEM images of the NVPF nanopieces from nanoflowers. **b** Charge/discharge profiles and **c** cycling capability of the NVPF nanoflowers [125]. Copyright 2016, Royal Society of Chemistry. **d** TEM images and **e** cycling performance of the NVPF 3D graphene conductive network [126]. Copyright 2017, American Chemical Society.

Element doping can also improve the performance of NVPF [128, 129]. Liu et al. [130] prepared NVPF by a sol-gel method and partially replaced the V position with the Y element. It was found that the improvement in electrochemical performance required an appropriate amount of Y doping, and the obtained $Na_3V_{1.9}Y_{0.1}(PO_4)_2F_3/C$ could give an optimal electrochemical performance with a specific capacity of approximately 80 mAh g^{-1} at 50C, which was higher than the 17 mAh g^{-1} of $Na_3V_2(PO_4)_2F_3/C$ materials. The enhanced electrochemical performance was attributed to an increase in electronic conductivity and the fast migration of Na^+ ions. Yi et al. [128] doped Ti into the crystal lattice of NVPF and investigated its influence on the electrochemical performance by controlling the Ti doping content and valence

state, as shown in **Fig. 13a-b.** Doping different valence states and different contents of Ti can induce different influences on the electrochemical performance of NVPF. When doped with Ti^{4+} (0.1 mol ratio), the obtained NVPF-Ti^{4+} shows both excellent specific capacity and rate capability during the charge and discharge processes. The improvement in electrochemical performance is mainly because doping a small amount of Ti can inhibit the growth of NVPF particles during the high-temperature sintering process and reduce the particle size. Additionally, it can be seen from **Fig. 13c** that the band gap is reduced by 0.118 eV, indicating that the electrons in the Ti-doped NVPF more easily transfer from the valence band to the conduction band. Therefore, Ti doping can effectively improve the intrinsic electron conductivity in bulk NVPF, leading to the improved electrochemical performance of NVPF.

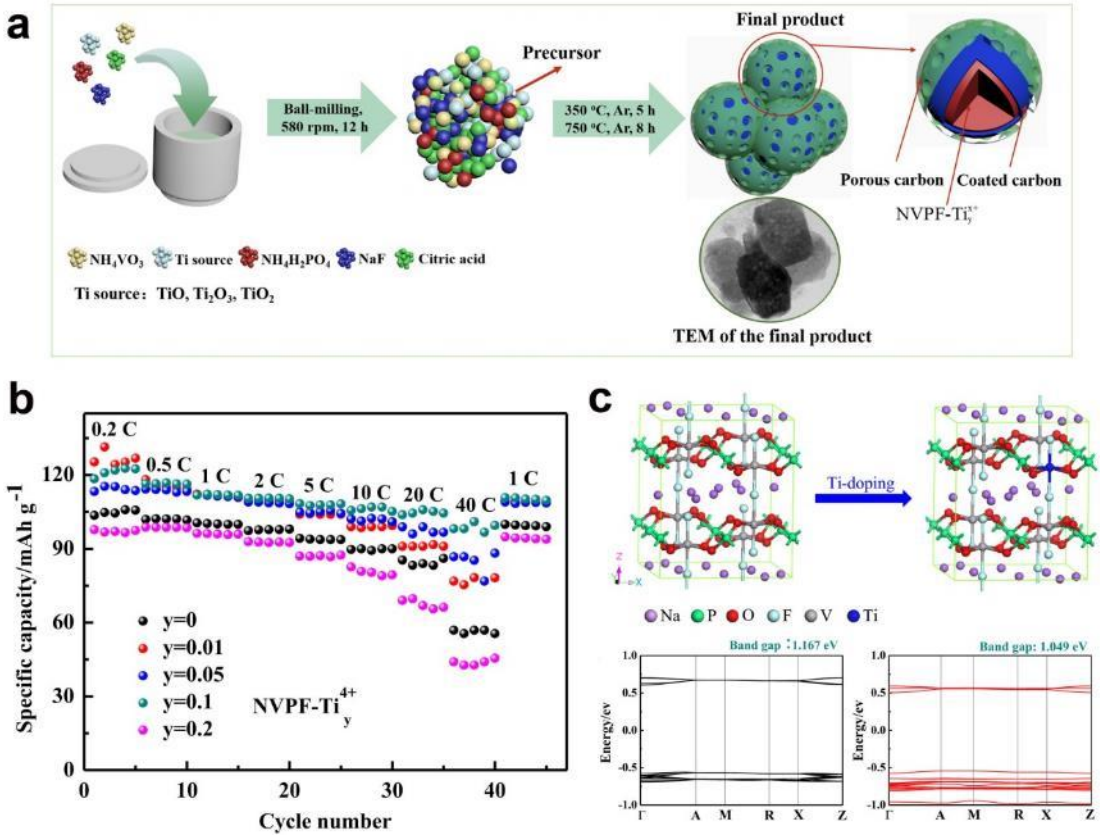

Fig. 13 a Schematic illustration showing the synthesis of NVPF-Ti_y^{z+} samples, **b** rate performance of NVPF-Ti^{4+}, and **c** crystal structure model of pristine and Ti-doped NVPF along with the band structures of pristine (left) and Ti-doped NVPF (right) [128]. Copyright 2018, Elsevier.

2.3.3 NASICON-type $Na_3V_2(PO_4)_2O_2F$ cathode material

According to the literature [131], F in $Na_3V_2(PO_4)_2F_3$ can be replaced by O, forming $Na_3V_2(PO_4)_2O_2F$ (NVOPF). As identified, a lower F content demonstrates weaker inductive effects, which facilitates Na^+ ion diffusion and reduces the polarization of the cathode [132]. As shown in **Fig. 14a,** $[V_2O_{10}F]$ bioctahedra (*i.e.*, two $[VO_5F]$ octahedra corners-sharing one F atom) are bridged by $[PO_4]$ tetrahedra to form a layered structure with Na^+ ions intercalated between these layers in the lattice structure of $Na_3V_2(PO_4)_2O_2F$ [133]. The crystal structure of NVOPF was studied in detail by Nguyen et al. [134]. They pointed out that NVOPF was well indexed in the I4/mmm space group and contained a fully occupied Na1 site and a half-occupied Na2 site with a distance of 2.374 Å between the two closest Na2 sites. By adjusting the oxygen content, the multielectron transfer of vanadium in the redox reaction could be realized. The partial oxygen substitution for fluorine could lead to the oxidation of V^{3+} to V^{4+} and form strong covalent vanadyl-type bonds. This can be confirmed by **Fig. 14b**. The $[V^{4+}O_5F]$ unit can be formed when y'=2 (y' represents the oxygen content) [134].

The phase transition process and mechanism of the NVOPF cathode during the charging/discharging processes were investigated and analyzed by time-resolved in

situ synchrotron XRD data. Sharma et al. [131] pointed out that in the initial course of the charging process, distinct evidence of a two-phase transition existed, which was consistent with the characteristics of the first or lower potential plateau during the charging profile (**Fig. 14c**). The phase transition process and mechanism of $Na_3V_2O_2(PO_4)_2F$ during the charging and discharging processes is shown in **Fig. 14c-f**. It can be concluded that in the course of the charging process, an initial solid solution of phase P (the sodium-rich phase) and two two-phase regions, including the phase transition process of P to P'(less sodium-poor phase) and P' to P'' (more sodium-poor phase), are related to most of the lower voltage plateau; additionally, an extended solid-solution region of the P'' phase (the higher potential plateau) and another two-phase reaction before the charged process is finished (or P‴ phase) is observed. The phase transition process and mechanism of the discharging process are obviously different; notably, the solid-solution processes and two-phase reaction behavior are involved but at markedly different points. The discharging process specifically includes a solid-solution P‴ phase at the higher potential plateau, a two-phase reaction during the transition from the higher to lower potential, and a solid-solution reaction and two two-phase reactions for the lower potential plateau before attaining the discharged state (P). Therefore, there exists an asymmetric process in the structural evolution of the cathode during charging and discharging. Notably, the main structure remains unchanged in the course of all the related reactions. However, during the phase transition process, the content and distribution of sodium will change along with the phase transition even within the same structural framework. Therefore, the

change in sodium in NVOPF can directly reflect the electrochemical reaction process and structural change of the cathode.

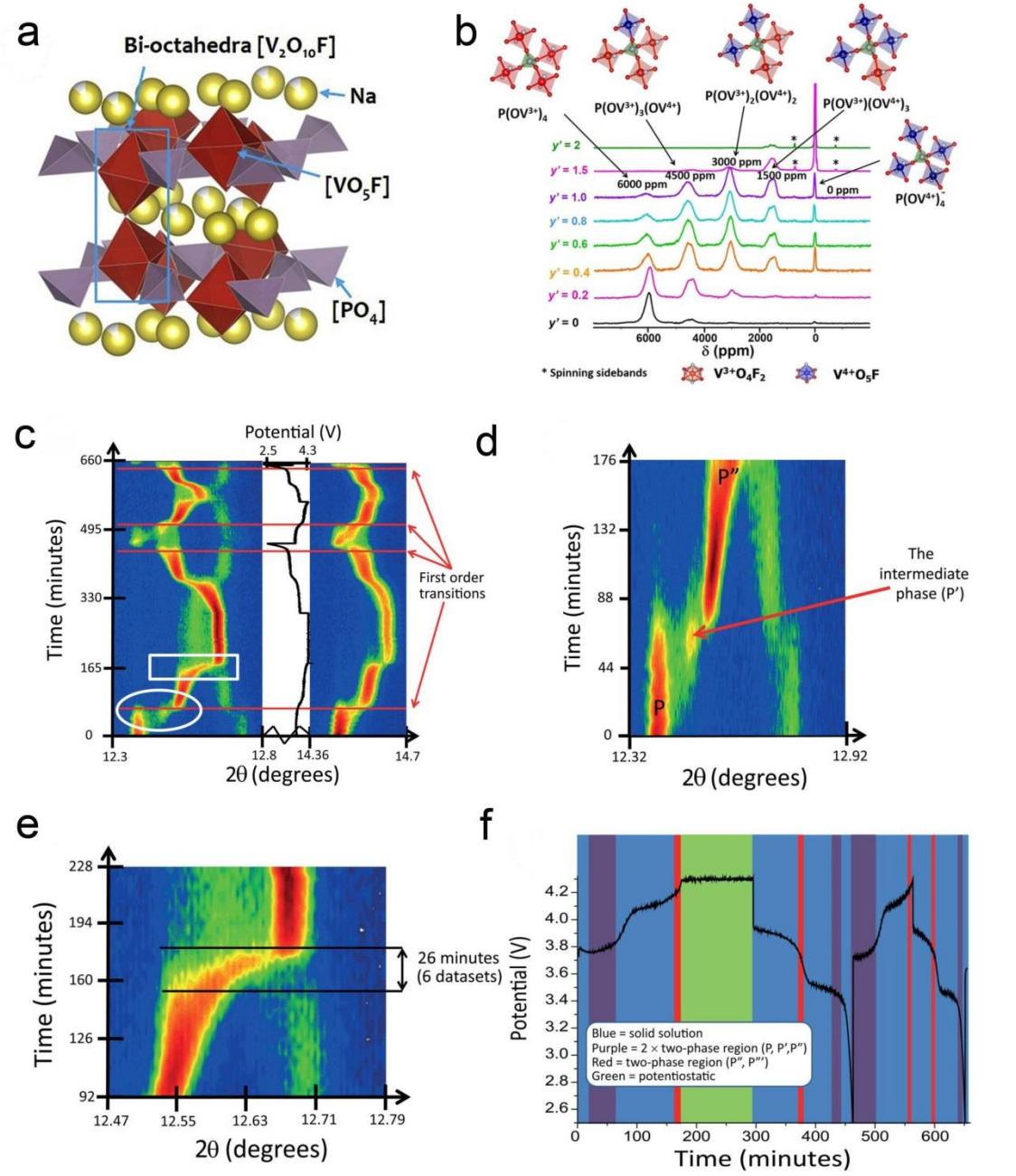

Fig. 14 a Crystalline structure of $Na_3V_2O_2(PO_4)_2F$ (NVOPF) [133]. Copyright 2019, Elsevier. **b** Hahn echo ^{31}P MAS NMR spectra of the $Na_3V^{3+}_{2-y'}V^{4+}_{y'}(PO_4)_2F_{3-y'}O_{y'}$ ($0 \le y' \le 2$) samples [134]. Copyright 2019, American Chemical Society. **c** In situ synchrotron XRD data with selected 2θ regions from 12.3° to 14.7°, including the 220, 113 lattice planes (left) and 311, 222 lattice planes (right). **d** Magnified region from

12.32° to 12.92° and **e** magnified region from 12.47° to 12.79°. **f** Reaction mechanism evolution of the $Na_{3-y}V_2O_2(PO_4)_2F$ electrode over the course of charging/discharging [131]. Copyright 2014, American Chemical Society.

Although NVOPF has a high theoretical capacity (~130 mAh g^{-1}), it also has the same low conductivity problem as NVP and NVPF. To improve its conductivity, various strategies have been widely studied, such as designing novel electrode structures, compounding with graphitized carbon materials, and optimizing the preparation process on a large scale. For example, Chao et al. [87] employed 2D geometry in a 3D architecture by reconfiguring the electrode material. A 3D matrix of electrode material configured in an appropriate geometry can deliver an improvement in power density and long-term cycling by shortening the ion transport distance and increasing the electronic conductivity; furthermore, the energy density can be improved by enhancing the mass loading per unit area. A 3D single-crystalline NVOPF array was prepared by using a VO_2 array as a seed layer on graphene foam (GF), as shown in **Fig. 15a**. The realized GF-NVOPF cathode electrode composed of 3D arrays shows flexible self-support, high rate performance and long cycle life characteristics. As shown in **Fig. 15b-c**, the electrochemical tests show that the GF-NVOPF cathode shows both high rate performance (charge/discharge in 60 s) and a long cycle life (10000 cycles at 50C) for Na^+ ion storage.

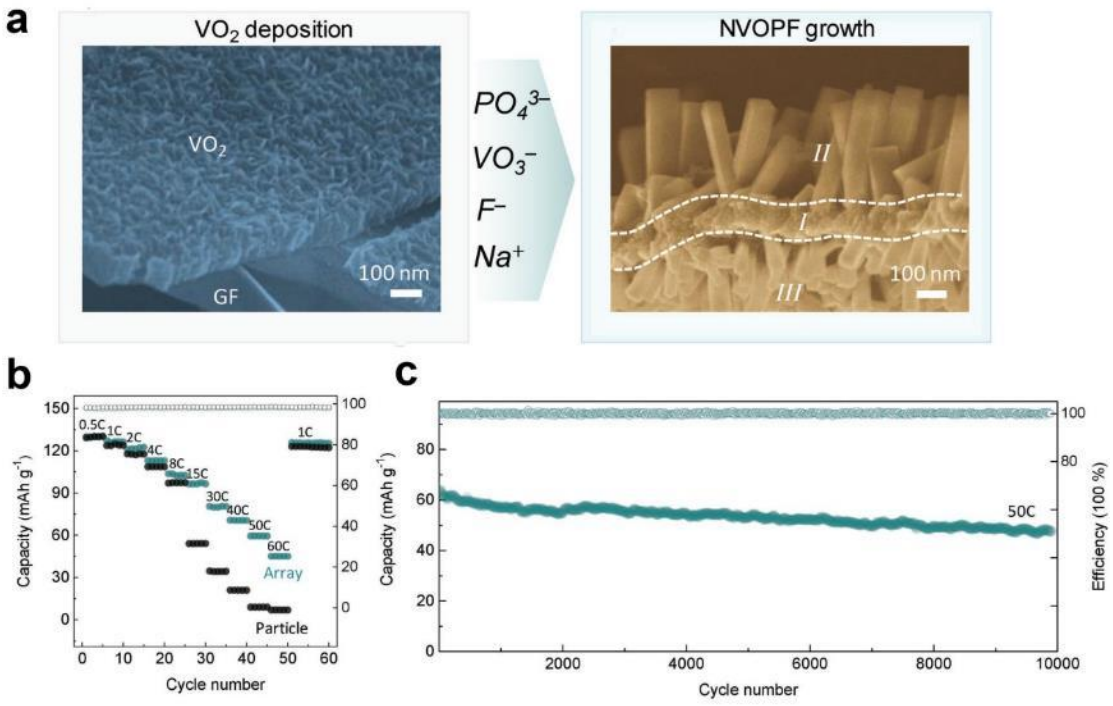

Fig. 15 a SEM images of the GF-VO_2 nanosheet seed layer precursor and GF-NVOPF array electrode. **b** Rate performance of the GF-NVOPF array. **c** Long-term cycling performance of the GF-NVOPF array electrodes at 50C [87]. Copyright 2018, WILEY-VCH.

In general, graphitized carbon materials have good electrical conductivity. By combining NVOPF with graphitized carbon, enhanced electrochemical performance can be realized. For example, Yin et al. [136] constructed a robust NVOPF/rGO microsphere composite via a spray-drying method and subsequent calcination process. As shown in **Fig. 16a**, the well-crystallized NVOPF particles are uniformly embedded in the three-dimensional graphene framework. As a result, the obtained NVOPF/rGO can deliver a high reversible rate performance (**Fig. 16b-c**) and shows superior cycling performance with 83.4% capacity retention after 2000 cycles at 30C (**Fig. 16d**). These results reveal that the combination of electrode materials and graphitized carbon materials is an effective way to enhance the electrochemical performance of an

electrode.

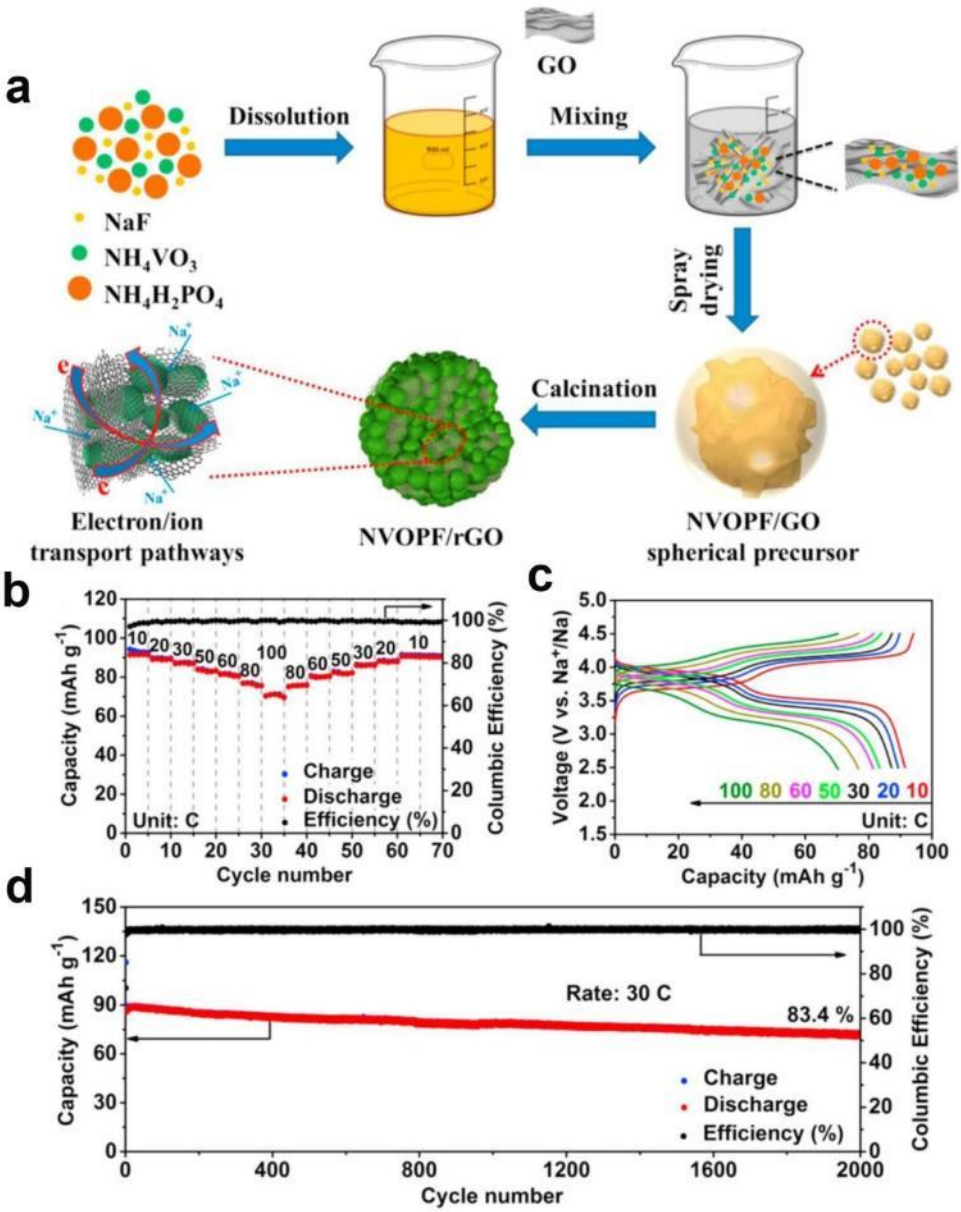

Fig. 16 a Synthesis process of the NVOPF/rGO microsphere composite. **b** High rate performance and **c** corresponding charge-discharge curves. **d** Long-term cycling performance of NVOPF at 30C [136]. Copyright 2017, Elsevier.

Most electrode materials are difficult to widely use because of the cost limitations in electric vehicles and energy storage systems. Therefore, the preparation process of

electrode materials needs optimization in terms of their large-scale manufacture. Qi et al. [137] proposed a facile one-step room-temperature strategy, with integrated extraction-separation and material-preparation, for the scalable fabrication of NVPOF multishelled microspheres to further reduce the cost, as shown in **Fig. 17a-b**. An enhanced electrochemical performance could also be achieved based on the large specific surface area corresponding to more electrochemical reaction sites and short diffusion paths for both ions and electrons. Impressively, the NVPOF multishelled microspheres were self-assembled by nanocrystals. In addition, superior Na-storage performance could be achieved without any additional high-temperature sintering, nanosizing, or carbon coating. As shown in **Fig. 17c**, the prepared NVPOF exhibits superior rate performance, displaying a discharge capacity of 81 mAh g^{-1} at 15C and retaining 70% of its initial capacity after 3000 cycles. This is probably the first time that NVPOF microspheres can be fabricated by a fast, facile, and controllable large-scale room-temperature synthesis method, showing great practical significance; furthermore, this method can also be applied to the preparation of other materials.

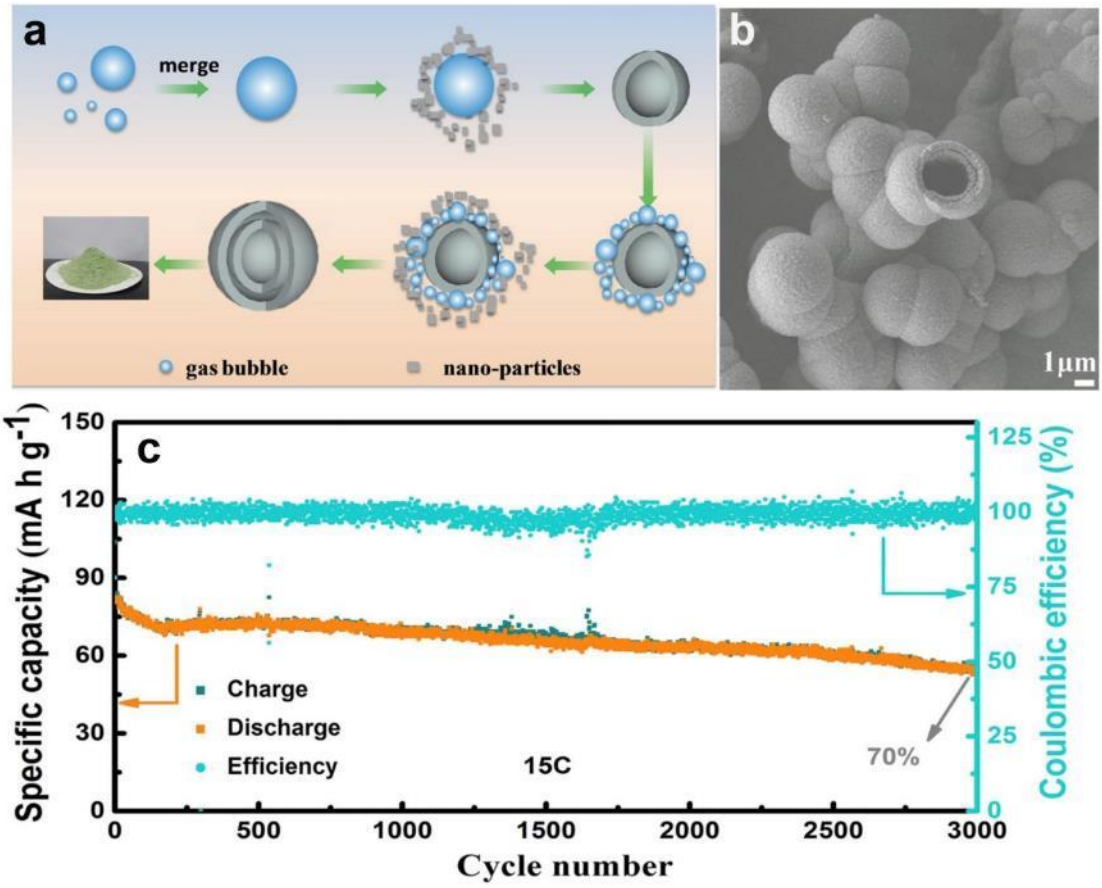

Fig. 17 a Possible self-assembly formation mechanism of NVPOF microspheres. **b** SEM image of multishelled NVPOF microspheres. **c** Cycling performance of the NVPOF electrode at 15C [137]. Copyright 2018, Elsevier.

2.4 Other NASICON cathode materials

Except for NVP, NVPF and NVOPF cathode materials, many other interesting materials conform to the chemical formula $Na_xMM'(XO_4)_3$ (M or M' = V, Fe, etc., X = P, S, x = 0~4), for instance, $NaVPO_4F$, $Na_2TiFe(PO_4)_3$, and $Na_3Fe_2(PO_4)_3$ [116, 138, 139]. Among these cathode materials, Fe-based NASICON cathode materials have been studied relatively more often because of their abundant valence states and multielectron reaction mechanism [140, 141]. The representative material is $Na_3Fe_2(PO_4)_3$ (NFP), which has a crystal structure similar to that of NVP. It also has the properties of a stable structure with low electronic conductivity, similar to all other

NASICON-structured materials. In this regard, carbon coating is commonly used to improve electron conductivity [142, 143]. For example, Rajagopalan et al. [144] prepared NFP cathode materials by carbon coating (SIP-C) with a simple solid-phase method, as shown in **Fig. 18a-b**. The charge transfer resistance (R_{ct}) of this material can be represented by the Nyquist plots shown in **Fig. 18c.** The results show that SIP-C has the smallest semicircle, suggesting it has the lowest R_{ct} value and enhanced electronic conductivity compared to SIP. Therefore, SIP-C has an excellent cycle life with an initial discharge capacity of 96 mAh g^{-1} at 1C; additionally, its capacity retention can reach 96%.

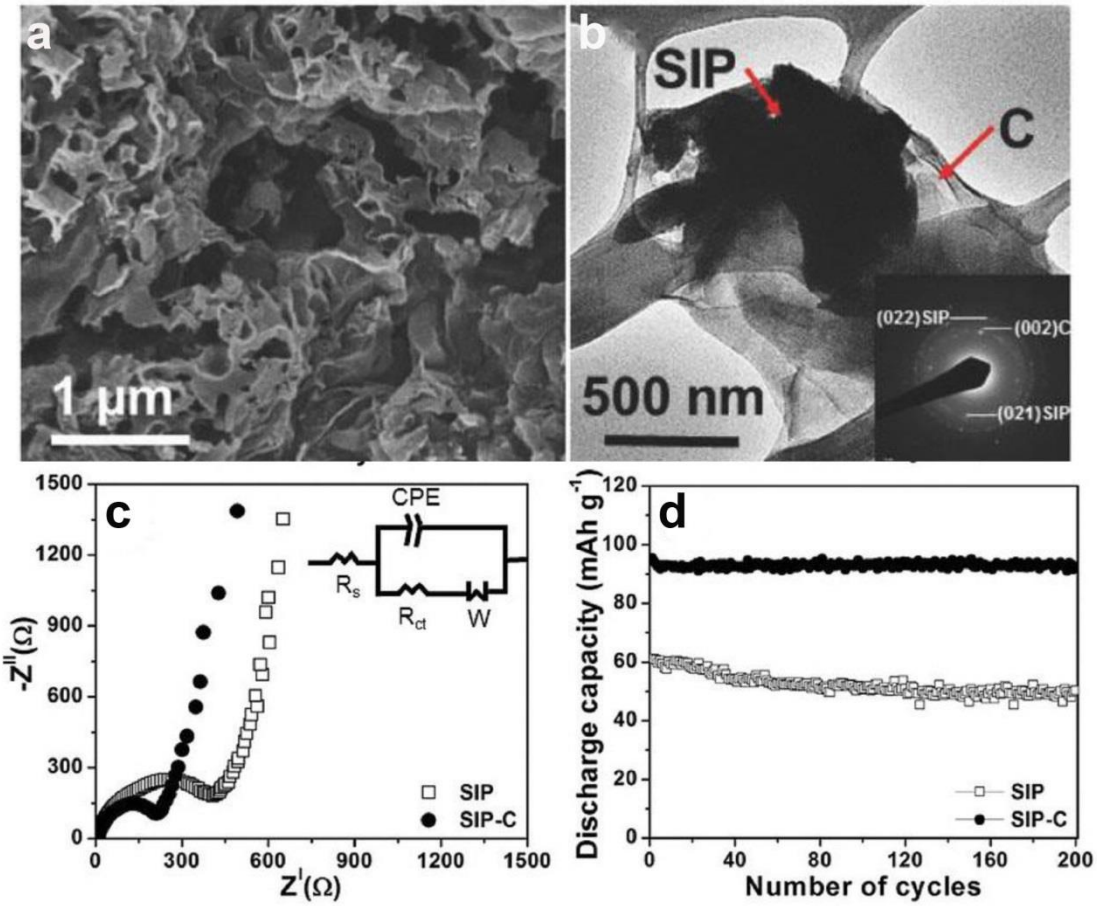

Fig. 18 a SEM image and **b** TEM image of SIP-C. **c** Nyquist plots (inset: the equivalent circuit) and **d** cycling performance of the SIP and SIP-C electrodes at 1C [144]. Copyright 2017, WILEY-VCH.

In summary, the relevant electrochemical performance of the discussed NASICON cathode materials are listed in **Table 1** for comparison.

Table. 1 Comparison of NASICON-type cathode materials in terms of storage properties.

Electrode material	Rate performance		Cycle performance		*Ref.*
	Capacity (mAh g^{-1})	Rate	Capacity retention	Cycle number	
NVP@C-GF	56	200C	91%	1000 cycles at 50C	[80]
NVP@C-CC	69.9	200C	82%	2000 cycles at 20C	[113]
PCL-NVP	83	20C	94.4%	4500 cycles at 10C	[145]
NVP@C@rGO	86	100C	64%	10000 cycles at 100C	[78]
NVP@NC/CC	80.	50C	81%	5000 cycles at 20C	[57]
NVP@C/MWCNT	63.2	80C	95.3%	5000 cycles at 20C	[146]
3D graphene-capped NVP-NFs	75.9	200C	62.5%	30000 cycles at 50C	[147]
CNT-decorated NVP	91.2	20C	92.6%	150 cycles at 10C	[79]
NVP@C	72	40C	82.8%	1000 cycles at 1C	[148]
Nano-NVP@pC	45.7	100C	89.5%	1000 cycles at 10C	[55]
PL-NVP@C	92	50C	91.3%	2000 cycles at 10C	[149]
NVP@C	101.77	30C	88%	700 cycles at 30C	[150]
$Na_3V_{2-x}Ca_x(PO_4)_3$@C	93	500C	93%	1000 cycles at 1C	[151]
NVP@C+N@CNTs	70	70C	88%	700 cycles at 5C	[77]
$Na_3V_{1.95}Mg_{0.05}(PO_4)_3$/C	94.2	30C	81%	50 cycles at 20C	[88]
NVP@C microspheres	96	30C	80%	5000 cycles at 10C	[152]
HP-NVP@SC	95	30C	91%	2500 cycles at 20C	[153]
NVP/GO	70.1	30C	86%	300 cycles at 5C	[154]
NVP@C	80	50C	78%	3000 cycles at 50C	[155]
NVP/CGO	70.4	20C	95%	1000 cycles at 2C	[74]
NVP@rGO	80	100C	71%	10000 cycles at 30C	[156]

NVP@C-NS-FL	77	80C	84.4%	1000 cycles at 100C	[157]
NVP@C–N150	71	80C	91%	5000 cycles at 20C	[62]
NVPF@C fibers	78.9	30C	81.8%	2000 cycles at 20C	[158]
NVPF@C@NCNT	76	100C	55%	1500 cycles at 40C	[159]
NVPF@C_D	116	10C	41%	5000 cycles at 100C	[160]
NVPF microcubes	71	20C	69%	2000 cycles at 20C	[127]
NVPF@rGO	95	30C	71%	5000 cycles at 20C	[161]
NVPF nanoparticles	74	15C	28.5%	5000 cycles at 30C	[162]
NVPF-SWCNT	100.7	10C	96.7%	500 cycles at 10C	[163]
NVPF@C nanoparticles	64	70C	60.8%	4000 cycles at 30C	[164]
NVPOF@P/N/C	128	0.5C	118.7%	100 cycles at 0.5C	[165]
NVOPF array	80	30C	56.7%	10000 cycles at 50C	[87]
RuO_2-coated NVOPF nanowires	105	20C	95%	1000 cycles at 20C	[166]
$Na_3(VO_{0.5})_2(PO_4)_2F_2$/graphene	82	20C	51%	1000 cycles at 51C	[167]
NVOPF@C nanocuboids	70	45C	56.7%	1000 cycles at 45C	[132]
NVPOF particles	85.9	20C	105.8%	500 cycles at 1C	[168]
NVOPF microsphere	81	15C	56.7%	3000 cycles at 15C	[137]
$Na_3V_2(PO_4)_2O_{1.6}F_{1.4}$	77.3	30C	81%	1000 cycles at 5C	[169]
Ru-doped NVOPF	102.5	20C	55%	7500 cycles at 20C	[170]
NVOPF cuboid arrays	56	20C	66%	500 cycles at 5C	[171]
NVOPF/rGO	95	100C	77%	1000 cycles at 20C	[172]
$Na_3Fe_2(PO_4)_3$	23	5C	54%	200 cycles at 1C	[142]
MCNT-reinforced $Na_3Fe_2(PO_4)_3$	101	0.1C	96%	500 cycles at 0.1C	[173]
Porous $Na_3Fe_2(PO_4)_3$	90.2	0.1 A g^{-1}	71.5%	1000 cycles at 0.5 A g^{-1}	[174]

3. Conclusion and perspectives

In summary, as one of the most promising alternatives to LIBs, SIBs have attracted increasing attention for use in next-generation high-energy batteries. Among reported SIB cathode materials, NASICON-type materials impressively demonstrate a stable structural framework and high ionic conductivity, showing promising application prospects.

In this review, based on the crystal structures of NASICON-type cathode materials, we summarized the research progress regarding the modification methods for improving material conductivity and electrochemical performance. The following strategies are used to obtain high-performance NASICON-based SIB cathode materials: (1) carbon coating and combining with carbon-based materials to improve the electronic conductivity of NASICON cathode materials; (2) exploring innovative synthesis methods to synthesize cathode materials with small particle sizes to improve the diffusion rate of ions; (3) realizing multielectron transfer in the electrochemical reaction by element doping; and (4) replacing anions to obtain a cathode material with a higher working voltage and more stable structure.

Although SIBs have progressed rapidly in recent years, there are still some remaining unresolved challenges that are still keeping SIBs far from commercialization. These challenges are summarized as follows:

(1) *Insufficient material synthesis methods, especially for large-scale production.* The current research remains mainly at the laboratory scale, and the main challenge is how to expand NASICON-type cathode materials from laboratory-scale research to industrially compatible production. One of the challenges involved in this process is probably due to the currently used material preparation methods, namely, the solid-phase, hydrothermal, freeze-drying and spray-drying methods. These methods

need a long production period while being expensive, showing insufficient efficiency and demonstrating high energy consumption during the annealing process. Thus, these methods limit the actual application of SIBs in large-scale energy storage and conversion systems. Therefore, it is urgent to explore more alternative strategies and develop an innovative preparation method that is inexpensive and easy to conduct along with demonstrating low energy consumption, and significantly improved material performance.

(2) *Insufficient fundamental understanding of the functional mechanisms of materials.* The detailed structural evolution and reaction mechanism of the multielectron reactions in NASICON cathode materials are still not fully understood. Therefore, the selection of cathode materials capable of conducting multielectron reactions is still limited. Thus, more theoretical calculations and in situ experimental characterization should be fully utilized to study the reaction mechanism, thereby promoting the adoption of effective strategies to enhance the electrochemical characteristics of existing materials and to find additional alternative materials.

(3) *Insufficient exploration of high-voltage electrolytes to realize multielectron transfer at high voltage with NASICON-based cathode materials.* Regarding this idea, some novel electrolytes that can be compatible with NASICON-based materials should be developed for high-performance SIBs in terms of energy/power densities and cycle life.

(4) *Insufficient design and fabrication of NASICON-based IB full cells for performance optimization.* The performance of SIBs is strongly affected by the battery design and configuration. At present, there are relatively few studies on SIB full cells. It seems that the traditional graphite anode is no longer suitable for SIB

systems. Therefore, it is particularly important to match NASICON-based cathode materials with suitable anode materials and safer and more cost-effective electrolytes.

(5) *Unoptimized operating conditions of NASICON-based cathode materials in SIBs.* Currently, NASICON-based cathode materials are mainly studied at room temperature, and their electrochemical reaction mechanisms and sodium-ion storage mechanisms at high or low temperatures have not been thoroughly studied. Therefore, further research is needed in this field.

Overall, it is certain that this type of NASICON-based cathode material should have good prospects in the field of SIBs in terms of their practical application in electrochemical energy storage systems.

4. Conflicts of interest

There are no conflicts of interest to declare.

5. Acknowledgments

This work is financially supported by the National Natural Science Foundation of China (Nos. 51602193, 21601122, 21905169), the Belt and Road Initiatives International Cooperation Project (No. 20640770300), the Shanghai ‘Chen Guang’ project (16CG63), the Shanghai Sailing Program (No. 18YF1408600), the Fundamental Research Funds for the Central Universities (WD1817002), the STFC Batteries Network (ST/R006873/1) and the EPSRC (EP/R023581/1, EP/P009050/1).

6. Notes and reference

1. Dunn, B., Kamath, H., Tarascon, J.M.: Electrical energy storage for the grid: a battery of choices. Science **334**, 928-935 (2011)
2. Baxter, J., Bian, Z., Chen, G., et al.: Nanoscale design to enable the revolution in renewable energy. Energy Environ. Sci. **2**, 559-588 (2009)
3. Kim, T.H., Park, J.S., Chang, S.K., et al.: The current move of lithium ion batteries towards the next phase. Adv. Energy Mater. **2**, 860-872 (2012)
4. Stamenkovic, V.R., Strmcnik, D., Lopes, P.P., et al.: Energy and fuels from electrochemical interfaces. Nat. Mater. **16**, 57-69 (2017)
5. Park, O.K., Cho, Y., Lee, S., Yoo, et al.: Who will drive electric vehicles, olivine or spinel? Energy Environ. Sci. **4**, 1621-1633 (2011)
6. Tender, L.M., Gray, S.A., Groveman, E., et al.: The first demonstration of a microbial fuel cell as a viable power supply: Powering a meteorological buoy. J. Power Sources **179**, 571-575 (2008)
7. Zhang, H.M., Lu, W.J., Li, X.F.: Progress and perspectives of flow battery technologies. Electrochem. Energy Rev. **2**, 492-506 (2019)
8. Lu, J.J., Yin, S.B., Shen, P.K.: Carbon-encapsulated electrocatalysts for the hydrogen evolution reaction. Electrochem. Energy Rev. **2**, 105-127 (2019)
9. Lokhande, P.E., Chavan, U.S., Pandey, A.: Materials and fabrication methods for electrochemical supercapacitors: overview. Electrochem. Energy Rev. **3**, 155-186 (2020)
10. Li, J.L., Daniel, C., Wood, D.: Materials processing for lithium-ion batteries. J. Power Sources **196**, 2452-2460 (2011)
11. Thackeray, M.M., Wolverton, C., Isaacs, E.D.: Electrical energy storage for transportation-approaching the limits of, and going beyond, lithium-ion batteries. Energy Environ. Sci. **5**, 7854-7863 (2012)
12. Wang, Q.S., Ping, P., Zhao, X.J., et al.: Thermal runaway caused fire and explosion of lithium ion battery. J. Power Sources **208**, 210-224 (2012)
13. Xiao, B.W., Sun, X.L.: Surface and subsurface reactions of lithium transition metal oxide cathode materials: an overview of the fundamental origins and remedying approaches. Adv. Energy Mater. **8**, 1802057 (2018)
14. Wang, L.L., Gu, X.L., Zhao, L.Y., et al.: ZnO@TiO_2 heterostructure arrays/carbon cloth by charge redistribution enhances performance in flexible anode for Li ion batteries. Electrochim. Acta **295**, 107-112 (2019)
15. Wang, L.L., Lu, B., Wang, S.S., et al.: Ultra-high performance of Li/Na ion batteries using N/O dual dopant porous hollow carbon nanocapsules as an anode. J. Mater. Chem. A **7**, 11117-11126 (2019)
16. Gur, T.M.: Review of electrical energy storage technologies, materials and systems: challenges and prospects for large-scale grid storage. Energy Environ. Sci. **11**, 2696-2767 (2018)
17. Li, M., Lu, J., Chen, Z.W., et al.: 30 years of lithium-ion batteries. Adv. Mater. **30**, 1800561 (2018)
18. Sun, W.W., Tang, X.X., Wang, Y.: Multi-metal-organic frameworks and their

derived materials for Li/Na-ion batteries. Electrochem. Energy Rev. **3**, 127-154 (2020)
19. Qian, J.F., Chen, Y., Wu, L., et al.: High capacity Na-storage and superior cyclability of nanocomposite Sb/C anode for Na-ion batteries. Chem. Commun. **48**, 7070-7072 (2012)
20. Sun, Q., Ren, Q.Q., Li, H., et al.: High capacity Sb_2O_4 thin film electrodes for rechargeable sodium battery. Electrochem. Commun. **13**, 1462-1464 (2011)
21. Xiong, H., Slater, M.D., Balasubramanian, M., et al.: Amorphous TiO_2 nanotube anode for rechargeable sodium ion batteries. J. Phys. Chem. Lett. **2**, 2560-2565 (2011)
22. Xiang, X.D., Lu, Y.Y., Chen, J.: Advance and prospect of functional materials for sodium ion batteries. Acta Chim. Sinica **75**, 154-162 (2017)
23. Fang, Y.J., Xiao, L.F., Chen, Z.X., et al.: Recent advances in sodium-ion battery materials. Electrochem. Energy Rev. **1**, 294-323 (2018)
24. Wang, T.Y., Su, D.W., Shanmukaraj, D., et al.: Electrode materials for sodium-ion batteries: considerations on crystal structures and sodium storage mechanisms. Electrochem. Energy Rev. **1**, 200-237 (2018)
25. Cao, Y.L., Xiao, L.F., Sushko, M.L., et al.: Sodium ion insertion in hollow carbon nanowires for battery applications. Nano Lett. **12**, 3783-3787 (2012)
26. Shen, W., Wang, C., Liu, H.M., et al.: Towards highly stable storage of sodium ions: a porous $Na_3V_2(PO_4)_3$/C cathode material for sodium-ion batteries. Chem. Eur. J. **19**, 14712-14718 (2013)
27. Hasa, I., Buchholz, D., Passerini, S., et al.: High performance $Na_{0.5}[Ni_{0.23}Fe_{0.13}Mn_{0.63}]O_2$ cathode for sodium-ion batteries. Adv. Energy Mater. **4**, 1400083 (2014)
28. Kubota, K., Asari, T., Yoshida, H., et al.: Understanding the structural evolution and redox mechanism of a $NaFeO_2$-$NaCoO_2$ solid solution for sodium-ion batteries. Adv. Funct. Mater. **26**, 6047-6059 (2016)
29. Takada, K., Sakurai, H., Takayama-Muromachi, et al.: A new superconducting phase of sodium cobalt oxide. Adv. Mater. **16**, 1901-1905 (2004)
30. Yoshida, H., Yabuuchi, N., Komaba, S.: $NaFe_{0.5}Co_{0.5}O_2$ as high energy and power positive electrode for Na-ion batteries. Electrochem. Commun. **34**, 60-63 (2013).
31. Yu, C.Y., Park, J.S., Jung, H.G., et al.: $NaCrO_2$ cathode for high-rate sodium-ion batteries. Energy Environ. Sci. **8**, 2019-2026 (2015)
32. Su, J.C., Pei, Y., Yang, Z.H., et al.: First-principles investigation on crystal, electronic structures and Diffusion barriers of $NaNi_{1/3}Co_{1/3}Mn_{1/3}O_2$ for advanced rechargeable Na-ion batteries. Comput. Mater. Sci **98**, 304-310 (2015)
33. Gong, Z.L., Yang, Y.: Recent advances in the research of polyanion-type cathode materials for Li-ion batteries. Energy Environ. Sci. **4**, 3223-3242 (2011)
34. Guo, S.P., Li, J.C., Xu, Q.T., et al.: Recent achievements on polyanion-type compounds for sodium-ion batteries: syntheses, crystal chemistry and electrochemical performance. J. Power Sources **361**, 285-299 (2017)
35. Zhang, B., Chen, H.Z., Tong, H., et al.: Synthesis and electrochemical performance of Ni doped $Na_3V_2(PO_4)_3$/C cathode materials for sodium ion

batteries. J. Alloys Compd. **728**, 976-983 (2017)
36. Li, C.Y., Wang, J.K., Wang, Y.J., et al.: Enhancing hydrogen evolution reaction by synergistically coupling NiMo alloy with $Ni(OH)_2$ nanosheet on carbon cloth. ChemistrySelect **5**, 6774-6779 (2020)
37. Li, H.X., Xu, M., Zhang, Z.A., et al.: Engineering of polyanion type cathode materials for sodium-ion batteries: toward higher energy/power density. Adv. Funct. Mater. **30**, 2000473 (2020)
38. Berthelot, R., Carlier, D., Delmas, C.: Electrochemical investigation of the P2-Na_xCoO_2 phase diagram. Nat. Mater. **10**, 74-80 (2011)
39. Han, H., Zhou, Z., Carozza, J.C., et al.: From lithium to sodium: design of heterometallic molecular precursors for the $NaMO_2$ cathode materials. Chem. Commun. **55**, 7243-7246 (2019)
40. Sauvage, F., Laffont, L., Tarascon, J.M., et al.: Study of the insertion/deinsertion mechanism of sodium into $Na_{0.44}MnO_2$. Inorg. Chem. **46**, 3289-3294 (2007)
41. Chen, S.Q., Wu, C., Shen, L.F., et al.: Challenges and perspectives for NASICON-type electrode materials for advanced sodium-ion batteries. Adv. Mater. **29**, 1700431 (2017)
42. Fang, Y.J., Zhang, J.X., Xiao, L.F., et al.: Phosphate framework electrode materials for sodium ion batteries. Adv. Sci. **4**, 1600392 (2017)
43. Jin, T., Li, H.X., Zhu, K.J., et al.: Polyanion-type cathode materials for sodium-ion batteries. Chem. Soc. Rev. **49**, 2342-2377 (2020)
44. Peng, M., Li, B., Yan, H., et al.: Ruthenium-oxide-coated sodium vanadium fluorophosphate nanowires as high-power cathode materials for sodium-ion batteries. Angew. Chem. Int. Ed. **54**, 6452-6456 (2015)
45. Xu, M.W., Wang, L., Zhao, X., et al.: $Na_3V_2O_2(PO_4)_2F$/graphene sandwich structure for high-performance cathode of a sodium-ion battery. Phys. Chem. Chem. Phys. **15**, 13032-13037 (2013)
46. Li, J.W., Cao, X.X., Pan, A.Q., et al.: Nanoflake-assembled three-dimensional $Na_3V_2(PO_4)_3$/C cathode for high performance sodium ion batteries. Chem. Eng. J. **335**, 301-308 (2017)
47. Cao, X.X., Pan, A.Q., Yin, B., et al.: Nanoflake-constructed porous $Na_3V_2(PO_4)_3$/C hierarchical microspheres as a bicontinuous cathode for sodium-ion batteries applications. Nano Energy **60**, 312-323 (2019)
48. Fang, J.Q., Wang, S.Q., Li, Z.T., et al.: Porous $Na_3V_2(PO_4)_3$@C nanoparticles enwrapped in three-dimensional graphene for high performance sodium-ion batteries. J. Mater. Chem. A **4**, 1180-1185 (2016)
49. Li, S.J., Ge, P., Zhang, C.Y., et al.: The electrochemical exploration of double carbon-wrapped $Na_3V_2(PO_4)_3$: towards long-time cycling and superior rate sodium-ion battery cathode. J. Power Sources **366**, 249-258 (2017)
50. Ling, R., Cai, S., Xie, D.L., et al.: Three-dimensional hierarchical porous $Na_3V_2(PO_4)_3$/C structure with high rate capability and cycling stability for sodium-ion batteries. Chem. Eng. J. **353**, 264-272 (2018)
51. Jian, Z.L., Yuan, C.C., Han, W.Z., et al.: Atomic structure and kinetics of NASICON $Na_xV_2(PO_4)_3$ cathode for sodium-ion batteries. Adv. Funct. Mater. **24**,

4265-4272 (2014)
52. Song, W.X., Ji, X.B., Wu, Z.P., et al.: First exploration of Na-ion migration pathways in the NASICON structure $Na_3V_2(PO_4)_3$. J. Mater. Chem. A **2**, 5358-5362 (2014)
53. Jian, Z.L., Han, W.Z., Lu, X., et al.: Superior electrochemical performance and storage mechanism of $Na_3V_2(PO_4)_3$ cathode for room-temperature sodium-ion batteries. Adv. Energy Mater. **3**, 156-160 (2012)
54. Duan, W.C., Zhu, Z.Q., Li, H., et al.: $Na_3V_2(PO_4)_3$@C core-shell nanocomposites for rechargeable sodium-ion batteries. J. Mater. Chem. A **2**, 8668-8675 (2014)
55. Zhu, Q.Z., Chang, X.Q., Sun, N., et al.: Confined growth of nano-$Na_3V_2(PO_4)_3$ in porous carbon framework for high-rate Na-ion storage. ACS Appl. Mater. Interfaces **11**, 3107-3115 (2018)
56. Zhao, L.N., Zhao, H.L., Long, X.Y., et al.: Superior high-rate and ultralong-lifespan $Na_3V_2(PO_4)_3$@C cathode by enhancing the conductivity both in bulk and on surface. ACS Appl. Mater. Interfaces **10**, 35963-35971 (2018)
57. Li, W., Yao, Z.J., Zhou, C.A., et al.: Boosting high-rate sodium storage performance of N-doped carbon-encapsulated $Na_3V_2(PO_4)_3$ nanoparticles anchoring on carbon cloth. Small **15**, 1902432 (2019)
58. Rafael, K., María José, A., Pedro, L., et al.: $Na_3V_2(PO_4)_3$/C nanorods with improved electrode-electrolyte interface as cathode material for sodium-ion batteries. ACS Appl. Mater. Interfaces **8**, 23151-23159 (2016)
59. Fang, Y.J., Xiao, L.F., Ai, X.P., et al.: Hierarchical carbon framework wrapped $Na_3V_2(PO_4)_3$ as a superior high-rate and extended lifespan cathode for sodium-ion batteries. Adv. Mater. **27**, 5895-5900 (2015)
60. Ren, W.H., Zheng, Z.P., Xu, C., et al.: Self-sacrificed synthesis of three-dimensional $Na_3V_2(PO_4)_3$ nanofiber network for high-rate sodium-ion full batteries. Nano Energy **25**, 145-153 (2016)
61. Jiang, Y., Yao, Y., Shi, J.N., et al.: One-dimensional $Na_3V_2(PO_4)_3$/C nanowires as cathode materials for long-life and high Rate Na-ion batteries. ChemNanoMat **2**, 726-731 (2016)
62. Yu, Y., Yao, Y., Jiang, Y., et al.: $Na_3V_2(PO_4)_3$ coated by N-doped carbon from ionic liquid as cathode materials for high rate and long-life Na-ion batteries. Nanoscale **9**, 10880-10885 (2017)
63. Jian, Z.L., Zhao, L., Pan, H.L., et al.: Carbon coated $Na_3V_2(PO_4)_3$ as novel electrode material for sodium ion batteries. Electrochem. Commun. **14**, 86-89 (2011)
64. Chen, L., Zhao, Y.M., Liu, S.H., et al.: Hard carbon wrapped $Na_3V_2(PO_4)_3$@C porous composite extending cycling lifespan for sodium-ion batteries. ACS Appl. Mater. Interfaces **9**, 44485-44493 (2017)
65. Liu, X.Y., Li, M.Y., Yang, X., et al.: Carbon encapsulation and chlorine doping enable $Na_3V_2(PO_4)_3$ superior sodium ion storage properties as cathode material for sodium ion battery. Powder Technol. **364**, 70-77 (2020)
66. Yao, X.H., Zhu, Z.X., Li, Q., et al.: 3.0 V high energy density symmetric sodium-ion battery: $Na_4V_2(PO_4)_3$ // $Na_3V_2(PO_4)_3$. ACS Appl. Mater. Interfaces **10**,

10022-10028 (2018)
67. Li, X., Huang, Y.Y., Wang, J.S., et al.: High valence Mo-doped $Na_3V_2(PO_4)_3$/C as a high rate and stable cycle-life cathode for sodium battery. J. Mater. Chem. A **6**, 1390-1396 (2017)
68. Zhu, Q.Z., Chang, X.Q., Sun, N., et al.: Microorganism-moulded pomegranate-like $Na_3V_2(PO_4)_3$/C nanocomposite for advanced sodium-ion batteries. J. Mater. Chem. A **5**, 9982-9990 (2017)
69. Jiang, Y., Zhang, H.C., Yang, H., et al.: $Na_3V_2(PO_4)_3$@nitrogen,sulfur-codoped 3D porous carbon enabling ultra-long cycle life sodium-ion batteries. Nanoscale **9**, 6048-6055 (2017)
70. Shen, W., Li, H., Wang, C., et al.: Improved electrochemical performance of the $Na_3V_2(PO_4)_3$ cathode by B-doping of the carbon coating layer for sodium-ion batteries. J. Mater. Chem. A **3**, 15190-15201 (2015)
71. Jiang, Y., Zhou, X.F., Li, D.J., et al.: Highly reversible Na storage in $Na_3V_2(PO_4)_3$ by optimizing nanostructure and rational surface engineering. Adv. Energy Mater. **8**, 1800068 (2018)
72. Dong, L., Liu, R.X., Feng, J.M., et al.: Improved high-rate performance of $Na_3V_2(PO_4)_3$ with an atomic layer deposition-generated Al_2O_3 layer as a cathode material for sodium-ion batteries. Mater. Lett. **205**, 75-78 (2017)
73. Rafael, K., Maciej, W., María, J.A., et al.: Improved surface stability of $C+M_xO_y$@$Na_3V_2(PO_4)_3$ prepared by ultrasonic method as cathode for sodium-ion batteries. ACS Appl. Mater. Interfaces **9**, 1471-1478 (2017)
74. Zhang, Y., Wu, M.M., Zhang, R.Y., et al.: A facile synthesis of monodispersed $Na_3V_2(PO_4)_3$ nanospheres anchored on cellular graphene oxide as a self-supporting cathode for high-rate sodium storage. ACS Appl. Energy Mater. **3**, 2867-2872 (2020)
75. Li, F.W., Chen, L., Knowles, G.P., et al.: Hierarchical mesoporous SnO_2 nanosheets on carbon cloth: a robust and flexible electrocatalyst for CO_2 reduction with high efficiency and selectivity. Angew. Chem. Int. Ed. **56**, 505-509 (2017).
76. Jung, Y.H., Lim, C.H., Kim, D.K.: Graphene-supported $Na_3V_2(PO_4)_3$ as a high rate cathode material for sodium-ion batteries. J. Mater. Chem. A **1**, 11350-11354 (2013)
77. Shen, W., Li, H., Guo, Z.Y., et al.: Double-nanocarbon synergistically modified $Na_3V_2(PO_4)_3$: an advanced cathode for high-rate and long-life sodium-ion batteries. ACS Appl. Mater. Interfaces **8**, 15341-15351 (2016)
78. Rui, X.H., Sun, W.P., Wu, C., et al.: An advanced sodium-ion battery composed of carbon coated $Na_3V_2(PO_4)_3$ in a porous graphene network. Adv. Mater. **27**, 6670-6676 (2015)
79. Chen, H.Z., Zhang, B., Wang, X., et al.: CNT-decorated $Na_3V_2(PO_4)_3$ microspheres as a high-rate and cycle-stable cathode material for sodium ion batteries. ACS Appl. Mater. Interfaces **10**, 3590-3595 (2018)
80. Zhong, X.W., Yang, Z.Z., Jiang, Y., Li, et al.: Carbon-coated $Na_3V_2(PO_4)_3$ anchored on freestanding graphite foam for high-performance sodium-ion cathodes. ACS Appl. Mater. Interfaces **8**, 32360-32365 (2016)

81. Jiang, Y., Yang, Z.Z., Li, W.H., et al.: Nanoconfined carbon-coated $Na_3V_2(PO_4)_3$ particles in mesoporous carbon enabling ultralong cycle life for sodium-ion batteries. Adv. Energy Mater. **5**, 1402104 (2015)
82. Liu, X.H., Feng, G.L., Wang, E.H., et al.: Insight into preparation of Fe-doped $Na_3V_2(PO_4)_3$@C from aspects of particle morphology design, crystal structure modulation, and carbon graphitization regulation. ACS Appl. Mater. Interfaces **11**, 12421-12430 (2019)
83. Wu, T., Sun, J.G., Yap, Z.Q.J., et al.: Substantial doping engineering in $Na_3V_{2-x}Fe_x(PO_4)_3$ ($0 \leqslant x \leqslant 0.15$) as high-rate cathode for sodium-ion battery. Mater. Des. **186**, 108287 (2020)
84. Klee, R., Lavela, P., Aragón, M.J., et al.: Enhanced high-rate performance of manganese substituted $Na_3V_2(PO_4)_3$/C as cathode for sodium-ion batteries. J. Power Sources **313**, 73-80 (2016)
85. Shen, W., Li, H., Guo, Z.Y., et al.: Improvement on high-rate performance of Mn-doped $Na_3V_2(PO_4)_3$/C as cathode materials for sodium ion batteries. RSC Adv. **6**, 71581-71588 (2016)
86. Zhang, J., Zhao, X.D., Song, Y.Z., et al.: Understanding the superior sodium-ion storage in a novel $Na_{3.5}Mn_{0.5}V_{1.5}(PO_4)_3$ cathode. Energy Storage Mater. **23**, 25-34 (2019)
87. Chao, D.L., Lai, C.H.M., Liang, P., et al.: Sodium vanadium fluorophosphates (NVOPF) array cathode designed for high-rate full sodium ion storage device. Adv. Energy Mater. **8**, 1800058 (2018)
88. Li, H., Yu, X.Q., Bai, Y., et al.: Effects of Mg doping on the remarkably enhanced electrochemical performance of $Na_3V_2(PO_4)_3$ cathode materials for sodium ion batteries. J. Mater. Chem. A **3**, 9578-9586 (2015)
89. Hu, Q., Liao, J.Y., He, X.D., et al.: In situ catalytic formation of graphene-like graphitic layer decoration on $Na_3V_{2-x}Ga_x(PO_4)_3$ ($0 \leqslant x \leqslant 0.6$) for ultrafast and high energy sodium storage. J. Mater. Chem. A **7**, 4660-4667 (2019)
90. Li, H., Bai, Y., Wu, F., et al.: Na-rich $Na_{3+x}V_{2-x}Ni_x(PO_4)_3$/C for sodium ion batteries: controlling the doping site and improving the electrochemical performances. ACS Appl. Mater. Interfaces **8**, 27779-27787 (2016)
91. Zhu, Q., Cheng, H., Zhang, X.M., et al.: Improvement in electrochemical performance of $Na_3V_2(PO_4)_3$/C cathode material for sodium-ion batteries by K-Ca co-doping. Electrochim. Acta **281**, 208-217 (2018)
92. Aragón, M.J., Lavela, P., Alcántara, R., et al.: Effect of aluminum doping on carbon loaded $Na_3V_2(PO_4)_3$ as cathode material for sodium-ion batteries. Electrochim. Acta **180**, 824-830 (2015)
93. María, J.A., Pedro, L., Gregorio, F.O., et al.: Benefits of chromium substitution in $Na_3V_2(PO_4)_3$ as a potential candidate for sodium-ion batteries. ChemElectroChem **2**, 995-1002 (2015)
94. Zhao, Y.J., Gao, X.W., Gao, H.C., et al.: Three electron reversible redox reaction in sodium vanadium chromium phosphate as a high-energy-density cathode for sodium-ion batteries. Adv. Funct. Mater. **30**, 1908680 (2020)
95. Qi, Y., Mu, L., Zhao, J., et al.: Superior Na-storage performance of

low-temperature-synthesized $Na_3(VO_{1-x}PO_4)_2F_{1+2x}$ $(0 \leqslant x \leqslant 1)$ nanoparticles for Na-ion batteries. Angew. Chem. Int. Ed. **54**, 9911-9916 (2015)
96. Serras, P., Palomares, V., Goñi, A., et al.: High voltage cathode materials for Na-ion batteries of general formula $Na_3V_2O_{2x}(PO_4)_2F_{3-2x}$. J. Med. Chem. **22**, 22301 (2012)
97. Chen, Y.J., Xu, Y.L., Sun, X.F., et al.: Preventing structural degradation from $Na_3V_2(PO_4)_3$ to $V_2(PO_4)_3$: F-doped $Na_3V_2(PO_4)_3$/C cathode composite with stable lifetime for sodium ion batteries. J. Power Sources **378**, 423-432 (2018)
98. Kosova, N.V., Rezepova, D.O.: Mixed sodium-lithium vanadium fluorophosphates $Na_{3-x}Li_xV_2(PO_4)_2F_3$: the origin of the excellent high-rate performance. J. Power Sources **408**, 120-127 (2018)
99. Qiu Ju, F., Kang, P., Zhen J.H., et al.: An investigation of $Li_{0.6}Na_{2.4}V_2(PO_4)_2F_3$ cathode with NASICON structure in lithium-ion battery. J. Power Sources **280**, 703-709 (2015)
100. Lim, S.J., Han, D.W., Nam, D.H., et al.: Structural enhancement of $Na_3V_2(PO_4)_3$/C composite cathode materials by pillar ion doping for high power and long cycle life sodium-ion batteries. J. Mater. Chem. A **2**, 19623-19632 (2014)
101. Zhou, G.M., Li, F., Cheng, H.M.: Progress in flexible lithium batteries and future prospects. Energy Environ. Sci. **7**, 1307-1338 (2014)
102. Liu, W., Song, M.S., Kong, B., et al.: Flexible and stretchable energy storage: recent advances and future perspectives. Adv. Mater. **29**, 1603436 (2017)
103. Chew, S.Y., Ng, S.H., Wang, J., et al.: Flexible free-standing carbon nanotube films for model lithium-ion batteries. Carbon **47**, 2976-2983 (2009)
104. David, L., Bhandavat, R., Singh, G.: MoS_2/Graphene composite paper for sodium-ion battery electrodes. ACS Nano **8**, 1759-1770 (2014)
105. Deng, Z.N., Jiang, H., Hu, Y.J., et al.: 3D ordered macroporous MoS_2@C nanostructure for flexible Li-ion batteries. Adv. Mater. **29**, 1603020 (2017)
106. Jiang, T., Bu, F.X., Feng, X.X., et al.: Porous Fe_2O_3 nanoframeworks encapsulated within three-dimensional graphene as high-performance flexible anode for lithium-ion battery. ACS Nano **11**, 5140-5147 (2017)
107. Liu, B., Zhang, J., Wang, X.F., et al.: Hierarchical three-dimensional $ZnCo_2O_4$ nanowire arrays/carbon cloth anodes for a novel class of high-performance flexible lithium-ion batteries. Nano Lett. **12**, 3005-3011 (2012)
108. Liu, S., Wang, Z., Yu, C., et al.: A flexible TiO_2(B)-based battery electrode with superior power rate and ultralong cycle life. Adv. Mater. **25**, 3462-3467 (2013)
109. Ma, K., Jiang, H., Hu, Y.J,et al.: 2D nanospace confined synthesis of pseudocapacitance-dominated MoS_2-in-Ti_3C_2 superstructure for ultrafast and stable Li/Na-ion batteries. Adv. Funct. Mater. **28**, 1804306 (2018)
110. Ma, K., Liu, Y., Jiang, H.,et al.: Multivalence-ion intercalation enables ultrahigh 1T phase MoS_2 nanoflowers to enhanced sodium-storage performance. CCS Chemistry **2**, 1472-1482 (2020)
111. Dong, Y.R, Zhu, Z.J, Hu, Y.J, et al.: Supersaturated bridge-sulfur and vanadium co-doped MoS_2 nanosheet arrays with enhanced sodium storage capability. Nano

Res. **14**, 74-80 (2021)
112. Xue, L., Zhang, Q.H., Zhu, X.H., et al.: 3D $LiCoO_2$ nanosheets assembled nanorod arrays via confined dissolution-recrystallization for advanced aqueous lithium-ion batteries. Nano Energy **56**, 463-472 (2019)
113. Guo, D.L., Qin, J.W., Yin, Z.G., et al.: Achieving high mass loading of $Na_3V_2(PO_4)_3$@carbon on carbon cloth by constructing three-dimensional network between carbon fibers for ultralong cycle-life and ultrahigh rate sodium-ion batteries. Nano Energy **45**, 136-147 (2018)
114. Liu, J., Tang, K., Song, K.P., et al.: Electrospun $Na_3V_2(PO_4)_3$/C nanofibers as stable cathode materials for sodium-ion batteries. Nanoscale **6**, 5081-5086 (2014)
115. Bianchini, M., Brisset, N., Fauth, F., et al.: $Na_3V_2(PO_4)_2F_3$ revisited: a high-resolution diffraction study. Chem. Mater. **26**, 4238-4247 (2014)
116. Le Meins, J.M., Crosnier-Lopez, M.P., Hemon-Ribaud, et al.: Phase transitions in the $Na_3M_2(PO_4)_2F_3$ family (M=Al^{3+}, V^{3+}, Cr^{3+}, Fe^{3+}, Ga^{3+}): synthesis, thermal, structural, and magnetic studies. J. Solid State Chem. **148**, 260-277 (1999)
117. Liu, Z.G., Hu, Y.Y., Matthew, T.D., et al.: Local structure and dynamics in the Na ion battery positive electrode material $Na_3V_2(PO_4)_2F_3$. Chem. Mater. **26**, 2513-2521 (2014)
118. Kuniko, C., Ayuko, K., Irina, D.G., et al.: Cathode properties of $Na_3M_2(PO_4)_2F_3$ [M=Ti, Fe, V] for sodium-ion batteries. J. Power Sources **227**, 80-85 (2012).
119. Shakoor, R.A., Seo, D.H., Kim, H., et al.: A combined first principles and experimental study on $Na_3V_2(PO_4)_2F_3$ for rechargeable Na batteries. J. Mater. Chem. **22**, 20535 (2012)
120. Bianchini, M., Fauth, F., Brisset, N., Weill, F., et al.: Comprehensive investigation of the $Na_3V_2(PO_4)_2F_3$-$NaV_2(PO_4)_2F_3$ system by operando high resolution synchrotron X-ray diffraction. Chem. Mater. **27**, 3009-3020 (2015)
121. Song, W.X., Cao, X.Y., Wu, Z.P., et al.: Investigation of the sodium ion pathway and cathode behavior in $Na_3V_2(PO_4)_2F_3$ combined via a first principles calculation. Langmuir **41**, 12438-12446 (2014)
122. Liu, S.Y, Cao, X.X, Zhang, Y.P, et al.: Carbon quantum dot modified $Na_3V_2(PO_4)_2F_3$ as a high-performance cathode material for sodium-ion batteries. J. Mater. Chem. A **8**, 18872-18879 (2020)
123. Ma, X.M, Cao, X.X, Zhou, Y.F,et al.: Tuning crystal structure and redox potential of NASICON-type cathodes for sodium-ion batteries. Nano Res. **13**, 3330-3337 (2020)
124. Song, W.X., Ji, X.B., Chen, J., et al.: Mechanistic investigation of ion migration in $Na_3V_2(PO_4)_2F_3$ hybrid-ion batteries. Phys. Chem. Chem. Phys. **17**, 159-165 (2014)
125. Qi, Y.R., Mu, L.Q., Zhao, J.M., et al.: pH-regulative synthesis of $Na_3(VPO_4)_2F_3$ nanoflowers and their improved Na cycling stability. J. Mater. Chem. A **4**, 7178-7184 (2016)
126. Zhu, C.B., Wu, C., Chen, C.C., et al.: A high power-high energy $Na_3V_2(PO_4)_2F_3$ sodium cathode: investigation of transport parameters, rational design and

realization. Chem. Mater. **29**, 5207-5215 (2017)
127. Cai, Y.S., Cao, X.X., Luo, Z.G., et al.: Caging $Na_3V_2(PO_4)_2F_3$ microcubes in cross-linked graphene enabling ultrafast sodium storage and long-term cycling. Adv. Sci. **5**, 1800680 (2018)
128. Yi, H.M., Ling, M.X., Xu, W.B., et al.: VSC-doping and VSU-doping of $Na_3V_{2-x}Ti_x(PO_4)_2F_3$ compounds for sodium ion battery cathodes: analysis of electrochemical performance and kinetic properties. Nano Energy **47**, 340-352 (2018)
129. Zhang, Y., Guo, S.R., Xu, H.Y.: Synthesis of uniform hierarchical $Na_3V_{1.95}Mn_{0.05}(PO_4)_2F_3$@C hollow microspheres as a cathode material for sodium-ion batteries. J. Mater. Chem. A **6**, 4525-4534 (2018)
130. Liu, W.Q., Yi, H.M., Zheng, Q., et al.: Y-Doped $Na_3V_2(PO_4)_2F_3$ compounds for sodium ion battery cathodes: electrochemical performance and analysis of kinetic properties. J. Mater. Chem. A **5**, 10928-10935 (2017)
131. Sharma, N., Serras, P., Palomares, V., et al.: Sodium distribution and reaction mechanisms of a $Na_3V_2O_2(PO_4)_2F$ electrode during use in a sodium-ion battery. Chem. Mater. **26**, 3391-3402 (2014)
132. Deng, G., Chao, D.L., Guo, Y.W., et al.: Graphene quantum dots-shielded $Na_3(VO)_2(PO_4)_2F$@C nanocuboids as robust cathode for Na-ion battery. Energy Storage Mater. **5**, 198-204 (2016)
133. Xu, J.L., Chen, J.Z., Tao, L., et al.: Investigation of $Na_3V_2(PO_4)_2O_2F$ as a sodium ion battery cathode material: Influences of morphology and voltage window. Nano Energy **60**, 510-519 (2019)
134. Nguyen, L.H.B., Camacho, P.S., Broux, T., et al.: Density functional theory-assisted ^{31}P and ^{23}Na magic-angle spinning nuclear magnetic resonance study of the $Na_3V_2(PO_4)_2F_3$-$Na_3V_2(PO_4)_2FO_2$ solid solution: unraveling its local and electronic structures. Chem. Mater. **31**, 9759-9768 (2019)
135. Nguyen, L.H.B. , Broux, T., Camacho, P.S., et al.: Stability in water and electrochemical properties of the $Na_3V_2(PO_4)_2F_3$-$Na_3(VO)_2(PO_4)_2F$ solid solution. Energy Storage Mater. **20**, 324-334 (2019)
136. Yin, Y.M., Xiong, F.Y., Pei, C.Y., et al.: Robust three-dimensional graphene skeleton encapsulated $Na_3V_2O_2(PO_4)_2F$ nanoparticles as a high-rate and long-life cathode of sodium-ion batteries. Nano Energy **41**, 452-459 (2017)
137. Qi, Y.R., Tong, Z.Z., Zhao, J.M., et al.: Scalable room-temperature synthesis of multi-shelled $Na_3(VOPO_4)_2F$ microsphere cathodes. Joule **2**, 2348-2363 (2018).
138. Essehli, R., Belharouak, I., Ben Yahia, H., et al.: Alluaudite $Na_2Co_2Fe(PO_4)_3$ as an electroactive material for sodium ion batteries. Dalton Trans. **44**, 7881-7886 (2015)
139. Sauvage, F., Quarez, E., Tarascon, J.M., et al.: Crystal structure and electrochemical properties vs. Na^+ of the sodium fluorophosphate $Na_{1.5}VOPO_4F_{0.5}$. Solid State Sci. **8**, 1215-1221 (2006)
140. Liu, Y., Zhou, Y.R., Zhang, J.X., et al.: Monoclinic phase $Na_3Fe_2(PO_4)_3$: synthesis, structure, and electrochemical performance as cathode material in sodium-ion batteries. ACS Sustainable Chem. Eng. **5**, 1306-1314 (2017)

141. Qiu, S., Wu, X.Y., Wang, M.Y., et al.: NASICON-type $Na_3Fe_2(PO_4)_3$ as a low-cost and high-rate anode material for aqueous sodium-ion batteries. Nano Energy **64**, 103941 (2019)
142. Zhou, J., Liu, X. J., Zhou, J. B.,et al.: Fully integrated hierarchical double-shelled Co_9S_8@CNT nanostructures with unprecedented performance for Li-S batteries. Nanoscale Horiz. **4**, 182-189 (2019)
143. Zhou, J. B., Liu, X. Y., Cai, W. L.,et al.: Wet-chemical synthesis of hollow red-phosphorus nanospheres with porous shells as anodes for high-performance lithium-ion and sodium-ion batteries. Adv. Mater. 29, 1700214 (2017).
144. Rajagopalan, R., Chen, B., Zhang, Z., et al.: Improved reversibility of Fe^{3+}/Fe^{4+} redox couple in sodium super ion conductor type $Na_3Fe_2(PO_4)_3$ for sodium-ion batteries. Adv. Mater. **29**, 1605694 (2017)
145. Zhang, J.W., Liu, W.F., Hu, H., et al.: An advanced blackberry-shaped $Na_3V_2(PO_4)_3$ cathode: assists in high-rate performance and long-life stability. Electrochim. Acta **292**, 736-741 (2018)
146. Chen, L., Zhong, Z.Q., Ren, S.B., et al.: Carbon-coated $Na_3V_2(PO_4)_3$ supported on multiwalled carbon nanotubes for half-/full-cell sodium-ion batteries. Energy Technol. **8**, 1901080 (2020)
147. Cao, X.X., Pan, A.Q., Liu, S.N., et al.: Chemical synthesis of 3D graphene-like cages for sodium-ion batteries applications. Adv. Energy Mater. **7**, 1700797 (2017)
148. Liu, X.H., Wang, E.H., Feng, G.L., et al.: Compared investigation of carbon-decorated $Na_3V_2(PO_4)_3$ with saccharides of different molecular weights as cathode of sodium ion batteries. Electrochim. Acta **286**, 231-241 (2018)
149. Wang, E.H., Xiang, W., Ranjusha, R., et al.: Construction of 3D pomegranate-like $Na_3V_2(PO_4)_3$/conducting carbon composites for high-power sodium-ion batteries. J. Mater. Chem. A **5**, 9833-9841 (2017)
150. Li, H., Wu, C., Bai, Y., Wu, F., et al.: Controllable synthesis of high-rate and long cycle-life $Na_3V_2(PO_4)_3$ for sodium-ion batteries. J. Power Sources **326**, 14-22 (2016)
151. Zhao, L.N., Zhao, H.L., Du, Z.H., et al.: Delicate lattice modulation enables superior Na storage performance of $Na_3V_2(PO_4)_3$ as both an anode and cathode material for sodium-ion batteries: understanding the role of calcium substitution for vanadium. J. Mater. Chem. A **7**, 9807-9814 (2019)
152. Lv, Z.Q., Ling, M.X., Yi, H.M., et al.: Electrode design for high-performance sodium ion batteries: coupling nanorod-assembled $Na_3V_2(PO_4)_3$@C microspheres with a 3D conductive charge transport network. ACS Appl. Mater. Interfaces **12**, 13869-13877 (2020)
153. Li, W., Yao, Z.J., Zhong, Y., et al.: Enhancement of the advanced Na storage performance of $Na_3V_2(PO_4)_3$ in a symmetric sodium full cell via a dual strategy design. J. Mater. Chem. A **7**, 10231-10238 (2019)
154. Tao, S., Wang, X., Cui, P., et al.: Fabrication of graphene-encapsulated $Na_3V_2(PO_4)_3$ as high-performance cathode materials for sodium-ion batteries. RSC Adv. **6**, 43591-43597 (2016)

155. Zheng, Q., Liu, W., Li, X., et al.: Facile construction of nanoscale laminated $Na_3V_2(PO_4)_3$ for a high-performance sodium ion battery cathode. J. Mater. Chem. A **4**, 19170-19178 (2016)
156. Li, F., Zhu, Y.E., Sheng, J.,et al.: GO-induced preparation of flake-shaped $Na_3V_2(PO_4)_3$@rGO as high-rate and long-life cathodes for sodium-ion batteries. J. Mater. Chem. A **5**, 25276-25281 (2017)
157. Zhou, Y.P., Zhang, X.H., Liu, Y.J., et al.: A high-temperature Na-ion battery: boosting the rate capability and cycle life by structure engineering. Small **16**, 1906669 (2020)
158. Li, Y., Liang, X., Zhong, G., et al.: Fiber-shape $Na_3V_2(PO_4)_2F_3$@N-doped carbon as a cathode material with enhanced cycling stability for Na-ion batteries. ACS Appl. Mater. Interfaces **12**, 25920-25929 (2020)
159. Wang, T.S., Zhang, W., Li, H.X., et al.: N-doped carbon nanotubes decorated $Na_3V_2(PO_4)_2F_3$ as a durable ultrahigh-rate cathode for sodium ion batteries. ACS Appl. Energy Mater. **3**, 3845-3853 (2020)
160. Liu, Q., Meng, X., Wei, Z.X., et al.: Core/double-shell structured $Na_3V_2(PO_4)_2F_3$@C nanocomposite as the high power and long lifespan cathode for sodium-ion batteries. ACS Appl. Mater. Interfaces **8**, 31709-31715 (2016).
161. Li, F., Zhao, Y.F., Xia, L.S., et al.: Well-dispersed $Na_3V_2(PO_4)_2F_3$@rGO with improved kinetics for high-power sodium-ion batteries. J. Mater. Chem. A **8**, 12391-12397 (2020)
162. Liu, Q., Wang, D.X., Yang, X., et al.: Carbon-coated $Na_3V_2(PO_4)_2F_3$ nanoparticles embedded in a mesoporous carbon matrix as a potential cathode material for sodium-ion batteries with superior rate capability and long-term cycle life. J. Mater. Chem. A **3**, 21478-21485 (2015)
163. Liu, S., Wang, L.B., Liu, J., et al.: $Na_3V_2(PO_4)_2F_3$-SWCNT: a high voltage cathode for non-aqueous and aqueous sodium-ion batteries. J. Mater. Chem. A **7**, 248-256 (2018)
164. Yao, Y., Zhang, L., Gao, Y., et al.: Assembly of $Na_3V_2(PO_4)_2F_3$@C nanoparticles in reduced graphene oxide enabling superior Na^+ storage for symmetric sodium batteries. RSC Adv. **8**, 2958-2962 (2018)
165. Zhang, L.L., Liu, J., Wei, C., et al.: N/P-dual-doped carbon-coated $Na_3V_2(PO_4)_2O_2F$ microspheres as a high-performance cathode material for sodium-ion batteries. ACS Appl. Mater. Interfaces **12**, 3670-3680 (2020)
166. Peng, M.H., Li, B., Yan, H.J., et al.: Ruthenium-oxide-coated sodium vanadium fluorophosphate nanowires as high-power cathode materials for sodium-ion batteries. Angew. Chem. Int. Ed. **54**, 6452-6456 (2015)
167. Xiang, X., Lu, Q., Han, M., et al.: Superior high-rate capability of $Na_3(VO_{0.5})_2(PO_4)_2F_2$ nanoparticles embedded in porous graphene through the pseudocapacitive effect. Chem. Commun. **52**, 3653-3656 (2016)
168. Gu, Z.Y., Guo, J.Z., Yang, Y., et al.: Precisely controlled preparation of an advanced $Na_3V_2(PO_4)_2O_2F$ cathode material for sodium ion batteries: the optimization of electrochemical properties and electrode kinetics. Inorg. Chem. Front. **6**, 988-995 (2019)

169. Li, C., Shen, M., Hu, B., et al.: High-energy nanostructured $Na_3V_2(PO_4)_2O_{1.6}F_{1.4}$ cathodes for sodium-ion batteries and a new insight into their redox chemistry. J. Mater. Chem. A **6**, 8340-8348 (2018)
170. Peng, M.H., Zhang, D.T., Zheng, L.M., et al.: Hierarchical Ru-doped sodium vanadium fluorophosphates hollow microspheres as a cathode of enhanced superior rate capability and ultralong stability for sodium-ion batteries. Nano Energy **31**, 64-73 (2017)
171. Mao, Z.F., Wang, R., He, B.B., et al.: Large-area, uniform, aligned arrays of $Na_3(VO)_2(PO_4)_2F$ on carbon nanofiber for quasi-solid-state sodium-ion hybrid capacitors. Small **15**, 1902466 (2019)
172. Zhang, Z.B., Chen, Z.H., Mai, Z.X., et al.: Toward high power-high energy sodium cathodes: a case study of bicontinuous ordered network of 3D porous $Na_3(VO)_2(PO_4)_2F$/rGO with pseudocapacitance effect. Small **15**, 1900356 (2019)
173. Xia, X.P., Cao, Y.J., Yao, L., et al.: MCNT-reinforced $Na_3Fe_2(PO_4)_3$ as cathode material for sodium-ion batteries. Arabian J. Sci. Eng. **45**, 143-151 (2020)
174. Cao, Y.J., Liu, Y., Chen, T., et al.: Sol-gel synthesis of porous $Na_3Fe_2(PO_4)_3$ with enhanced sodium-ion storage capability. Ionics **25**, 1083-1090 (2019)

Qingbo Zhou received his bachelor's degree from Hubei Engineering University, Hubei Province in 2018. At present, he is pursuing his Master of Engineering degree at Shanghai University of Engineering Science and collaborating on research at Shanghai University. His current research focuses on lithium-ion batteries and sodium-ion batteries.

Dr. Linlin Whang received her Ph.D. in inorganic chemistry in 2013 from the University of Science and Technology of China (USTC) under the direction of Prof. Kai-bin Tang and Prof. Yi-tai Qian. She was selected for the Shanghai Sailing Program in 2014. She is currently a full associate professor at Shanghai University. Her current focus is on advanced materials for electrochemical energy storage and conversion, including electrodes in Li/Na/K-ion batteries and electrocatalysis in fuel cells.

Dr. Wenyao Li received his Ph.D. in Material Physics and Chemistry from Donghua University (2014). He is an associate professor at Shanghai University of Engineering Science and visiting professor at University College London. He has authored and coauthored more than 80 refereed journal publications, has an H-index of 33, and holds over 20 patents. His current research interests focus on the preparation, characterization and application of low-dimensional nanomaterials and exploring the application of these nanomaterials in the new generation of energy storage devices.

Kangning Zhao currently holds a postdoctoral position at the Laboratory of Advanced Separations (LAS) in the School of Basic Science, École Polytechnique Fédérale de Lausanne (EPFL). He received his Ph.D. degree from Wuhan University of Technology in 2019, during which he carried out his visiting scholarly research in

the laboratory of Prof. Xudong Wang at the University of Wisconsin-Madison from 2016–2018. Currently, his research interest includes membranes for electrochemical catalysis and energy storage devices.

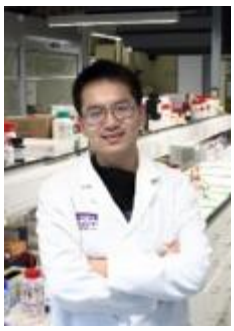

Dr. Guanjie He is a Senior Lecturer in Chemistry, University of Lincoln and an Honorary Lecturer in the Department of Chemistry and Department of Chemical Engineering, University College London (UCL). Dr. He received his Ph.D. from the Chemistry department at UCL and his BSc degree from Donghua University. Dr. He's research focuses on materials for electrochemical energy storage and conversion applications, especially electrode materials in aqueous electrolyte systems. Dr. He has published 70 papers in peer-reviewed journals, with a total citation of over 2300 and an H-index of 27 (Data from Google Scholar).

Prof. Ivan Parkin obtained his BSc and Ph.D. degrees from Imperial College London. He has published over 900 scientific journal papers, including Science, Nature Energy, Advanced (Functional, Energy) Materials, Nature Communications, and JACS, and has an H-index of 85. His groups are mainly concerned with the synthesis of new materials and coatings. He works extensively in chemical vapor deposition, nanoparticle synthesis, antimicrobial coatings, gas sensing, superhydrophobic surfaces and energy materials. Prof. Parkin is a member of Academia Europaea, a fellow of the Royal Society of Chemistry and has received multiple awards, such as the Tilden Medal, Griffith Medal and Beilby Medal.

Prof. Paul Shearing completed a Ph.D. in Imperial College London. He joined the Department of Chemical Engineering at UCL in 2011. In 2017, he was a founding investigator of the UK's Faraday Institution, where he chairs the Training & Diversity Panel and leads the £10 M LiSTAR program. In 2014, he was named the Institute of Chemical Engineers, Young Chemical Engineer of the Year in Academia, and in 2016, he was named the RAEng Engineers Trust Young Engineer of the Year. He has published more than 240 peer-reviewed papers in this area over the past 5 years and has delivered over 100 invited talks on 5 continents. His research makes extensive use of synchrotron radiation, and he has successfully conducted experiments at most of the world's major light sources.

Prof. Brett is the Chair of EIL in University College London (UCL). His research is in the area of electrochemical engineering and technology. This includes electrochemical energy conversion and storage (fuel cells, batteries, supercapacitors, electrolyzers), electrochemical sensors, electroanalysis, hybrid vehicles and microgeneration technologies. He has published over 530 scientific journal papers and has an H-index of 56. He specializes in developing novel diagnostic techniques for the study of high- and low-temperature fuel cells and their materials.

Dr. Jiujun Zhang is a Professor in the College of Sciences/Institute for Sustainable Energy at Shanghai University, a former Principal Research Officer at the National Research Council of Canada (NRC). Dr. Zhang is a Fellow of the Canadian Academy of Engineering (CAE), Fellow of

The Academy of Science of The Royal Society of Canada (FRSCCA), Fellow of The Engineering Institute of Canada (EIC), Fellow of the International Society of Electrochemistry (ISE), and Fellow of the Royal Society of Chemistry (RSC-UK). Dr. Zhang received his B.S. and M.Sc. in electrochemistry from Peking University in 1982 and 1985, respectively, and his Ph.D. in Electrochemistry from Wuhan University in 1988. Dr. Zhang's main research areas are electrochemistry, electrocatalysts, fuel cells, lithium batteries, metal-air batteries, supercapacitors, and H_2O/CO_2 electrolysis.

Prof. Xueliang (Andy) Sun is the Canada Research Chair in Development of Nanomaterials for Clean Energy, a Fellow of the Royal Society of Canada and Canadian Academy of Engineering and a Full Professor at the University of Western Ontario, Canada. Dr. Sun received his Ph.D. in materials chemistry in 1999 from the University of Manchester, UK, which he followed up by working as a postdoctoral fellow at the University of British Columbia, Canada, and as a Research Associate at L′ Institut National de la Recherche Scientifique (INRS), Canada. His current research interests are focused on advanced materials for electrochemical energy storage and conversion.